INDOOR LOCALIZATION AND RADIO MAP ESTIMATION USING GEOMETRICALLY PERTURBED UNSUPERVISED MANIFOLD ALIGNMENT

BY

KHAQAN MAJEED

A Thesis Presented to the
DEANSHIP OF GRADUATE STUDIES

KING FAHD UNIVERSITY OF PETROLEUM & MINERALS

DHAHRAN, SAUDI ARABIA

In Partial Fulfillment of the
Requirements for the Degree of

MASTER OF SCIENCE

In

ELECTRICAL ENGINEERING

MAY 2014

KING FAHD UNIVERSITY OF PETROLEUM & MINERALS
DHAHRAN 31261, SAUDI ARABIA

DEANSHIP OF GRADUATE STUDIES

This thesis, written by **KHAQAN MAJEED** under the direction of his thesis adviser and approved by his thesis committee, has been presented to and accepted by the Dean of Graduate Studies, in partial fulfillment of the requirements for the degree of **MASTER OF SCIENCE IN ELECTRICAL ENGINEERING**.

Thesis Committee

Dr. Sameh O. Sorour (Adviser)

Dr. Tareq Y. Al-Naffouri (Co-adviser)

Dr. Ali H. Muqaibel (Member)

Dr. Ali Ahmad Al-Shaikhi (Member)

Dr. Shahrokh Valaee (Member)

Dr. Ali Ahmad Al-Shaikhi
Department Chairman

Dr. Salam A. Zummo
Dean of Graduate Studies

1/6/14

Date

To my dearest Mom, Dad and wonderful siblings

ACKNOWLEDGMENTS

TABLE OF CONTENTS

LIST OF TABLES

LIST OF FIGURES

LIST OF ABBREVIATIONS

AoA   Angle-of-Arrival

AP   Access Point

BFGS algo   Broyden-Fletcher-Goldfarb-Shanno algorithm

CS   Compressed Sensing

GPS   Global Positioning System

HK   Heat Kernel

LAN   Local Area Network

LBS   Location-Based Services

LLE   Locally Linear Embedding

NN   Nearest Neighbor

PDA   Personal Digital Assistant

POI   Point Of Interest

RSS   Received Signal Strength

SMA   Semi-supervised Manifold Alignment

TDoA	Time-Difference-of-Arrival
ToA	Time-of-Arrival
UMA	Unsupervised Manifold Alignment
VoIP	Voice over IP
WLAN	Wireless Local Area Network
WNIC	Wireless Network Interface Controller

THESIS ABSTRACT

NAME:	Khaqan Majeed
TITLE OF STUDY:	Indoor Localization and Radio Map Estimation using Geometrically Perturbed Unsupervised Manifold Alignment
MAJOR FIELD:	Electrical Engineering
DATE OF DEGREE:	May, 2014

The main limitation of deploying/updating Received Signal Strength (RSS) based indoor localization system is the construction of fingerprinted radio map, which is quite a hectic and time-consuming process especially when the indoor area is enormous and/or dynamic. Different approaches have been undertaken to reduce such deployment/update efforts, but the performance degrades when the fingerprinting load is reduced below a certain level. In this work, we propose an indoor localization scheme that requires very small fraction of fingerprinting load (1% of total grid points, i.e. 2 in our case), some crowd sourced readings and plan coordinates of the indoor environment. The 1% fingerprinting load is used only to perturb the local geometries in the plan coordinates. Our proposed algorithm was shown to achieve less than 5m mean localization error with 1% fingerprint-

ing load and a limited number of crowd sourced readings, when other learning based localization schemes pass the 10m mean error with the same information. The performance is further improved by clustering the crowd sourced information where the few collected fingerprints act as cluster heads.

The few location estimations together with few fingerprints help to estimate the complete radio map of the indoor environment. The estimation of radio map does not demand extra workload rather it employs the already available information from the proposed indoor localization framework. The testing results for radio map estimation show almost 50% performance improvement by using the aforementioned information as compared to using only fingerprints.

ملخص الرسالة

الاسم الكامل: خاقان مجيد

عنوان الرسالة: تحديد المواقع الداخلية و توقع الخريطة الراديوية باستخدام المحاذاة المتشعبة الغير مراقبة المعدلة هندسيا.

التخصص: الهندسة الكهربائية

تاريخ الدرجة العلمية: مايو 2014

المحدد الرئيسي لتركيب\تحديث نظام تحديد الموقع بالاعتماد على قوة الإشارة المستلمة هو إنشاء بصمة بالخريطة الراديوية، و هو ما يعد مستعصيا و مستنزفا للوقت خصوصا عندما تكون المساحة الداخلية كبيرة و متغيرة. لقد استعملت عدة أساليب للتقليل من الجهود المبذولة في عملية التركيب\التحديث، لكن الانخفاض في الأداء عند تقليل عدد البصمات المأخوذة عن حد معين. في هذا العمل،نحن نقترح طريقة لتحديد المواقع الداخلية تحتاج نسبة قليلة من عدد البصمات الكلي (1% من عدد النقاط الكلي)، بعض القراءات متعددة المصادر، إضافة إلى إحداثيات البيئة الداخلية. نسبة الواحد بالمائة من عدد البصمات تستخدم لتغيير الإحداثيات. النتائج تظهر أن الخوارزمية المقترحة تحقق خطأ في تحديد الموقع أقل من 5 أمتار باستخدام 1% من البصمات المأخوذة و عدد محدود من القراءات متعددة المصادر، مقارنة بطرق أخرى تحقق نسبة خطأ أعلى من 10 أمتار بنفس كمية المعلومات. القليل من التقديرات بالإضافة إلى القليل من البصمات يساعد على توقع الخريطة الراديوية الكاملة للبيئة الداخلية. تقدير الخريطة الراديوية لا يتطلب المزيد من المعلومات المتوفرة من نظام تحديد المواقع المقترح. ظهر التجارب تحسنا في الأداء بينسبة 50% عن طريق استخدام المعلومات السابق ذكرها لامقارنة مع استخدام البصمات فقط.

CHAPTER 1

INTRODUCTION AND MOTIVATION

The advent of mobile devices (e.g. laptops, personal digital assistants (PDAs), smart phones, tablets) has aided a lot in the proliferation of location-based services (LBS). The LBS in outdoor applications include information sharing of personal visits (e.g. social networking), military purposes, vehicle navigation, marking Point of Interest (POI) (e.g. restaurants, hospitals, recreational parks, malls). The indoor applications include object detection, navigation in giant malls/buildings, guiding disabled persons in huge indoor areas, assisting students through university campus, etc. The localization, both indoor and outdoor, has very useful applications especially in way finding.

The Global Positioning System (GPS) offers suitable accuracy in outdoor location estimation applications but fails to provide satisfactory performance in indoor environments due to unpredictability of radio propagation. The signals from GPS

satellites become very weak while penetrating through buildings. Wireless Local Area Networks (WLANs) infrastructure using Received Signal Strength (RSS) has gained much importance recently over Angle-of-Arrival (AoA) and Time-of-Arrival (ToA)/Time-Difference-of-Arrival (TDoA) techniques due to hardware simplicity [1, 2]. Some of the other techniques make use of sensory measurements in users' mobile phones. The schemes employing Wi-Fi fingerprinting do not require any investment cost in deploying Access Points (APs), i.e. existing installed APs can be used for location estimation. Moreover, the mobile devices are widely available nowadays and are equipped with Wireless Network Interface Controller (WNIC) so there is no need for additional hardware changes. The indoor localization technique, proposed later in this work, does not require additional sensors present in the mobile phones as required by sensory measurement techniques. The signal strength values measured by mobile devices from Wi-Fi APs are employed in this work to perform indoor localization.

1.1   Wi-Fi based Positioning

The indirect self-positioning topology [3, 4] is considered in this work, in which the mobile unit receives signals from several APs present in the indoor area and sends the measurement results to the central computational unit. The server/central unit then estimates the position of the user based on the RSS measurements received from it. The estimated position is then sent to the mobile user via some wireless data link. The location sensing in WLANs using RSS is broadly divided

into three categories [3]. The brief description about these categories is following.

1. Obtaining the relationship between RSS value and position by using radio propagation models. The range is estimated theoretically or empirically based on the difference between the transmitted and received signals. The locations of APs need to be known in this case. The position of the mobile user is then estimated from the signal strength.

2. The mobile target is affiliated with a particular antenna among some group of antennas based on maximum signal strength. Here the location of APs (antennas) needs to be known in advance.

3. Location fingerprintng makes use of RSS values from concerned APs in the indoor environment. The RSS readings are obtained from all the concerned APs and stacked as a vector corresponding to a specific indoor position. The fingerprinting/radio map contains measurement vectors at all the grid points in the indoor environment.

The problem related with the first two options, mentioned above, is that the signal strength follows inverse square relationship with the distance (this is true in case of free space) and the variation of RSS values cannot be modeled as gaussian. The path loss occurs in radio propagation due to multi-path and other factors. The indoor environment is dynamic i.e. moving objects such as doors, windows, persons, escalators, elevators, etc are the major sources of signal strength variations in radio wave propagation. However, the third option, location fingerprinting, is the most preferred approach since it avoids the inaccuracies which occur in case

of employing radio propagation models. The fingerprint database (a.k.a the radio map) is the collection of RSS readings obtained from different APs at reference or grid points in an indoor area. In the most traditional scenario of this method, the localization problem is basically divided into two phases, the offline phase and the online phase. In the offline phase, the radio map is constructed by collecting the RSS fingerprints (a.k.a calibration data) at all grid points of the indoor environment. In the online phase, the localization requests are received and compared to the radio map to estimate their users' locations.

1.2 Motivation and Problems Targeted

According to the aforementioned details, the building of fingerprint database is quite hectic and time-consuming process since one has to obtain RSS readings at all the grid points in an indoor environment. The workload increases when the size of the indoor area under consideration increases. Keeping in view these facts, any efforts towards reducing the cost and workload consumed in building the radio map while maintaining the minimum error floor are of great practical importance. Some works [5–8] have reduced the fingerprinting load but the performance is severely effected when fingerprints are reduced below a certain number.

In [7], some RSS readings are collected at certain positions of the indoor area and are termed as labeled data. Localization requests are obtained in the online stage and are called unlabeled data. The labeled and unlabeled data are then aligned using semi-supervised manifold alignment (SMA) [9]. The positions are

estimated by closest match in the common lower dimensional manifold. The performance degrades when the number of fingerprints are reduced to a small value (10% of the total grid points in the indoor environment).

In this work, we aim to further reduce the fingerprinting load $(1-5\%)$ while still maintaining low degradation in performance. In this approach, the server collects a considerable number of crowd sourced RSS readings from the casual visitors of the environment. Nonetheless, we still require some very limited number of labeled positions (fingerprints) to perturb the geometry of coordinates since there is high symmetry in the coordinate plan. Indeed, it becomes difficult to differentiate between the small chunk of points from one place to another in an indoor area (will be explained in later chapters). These few fingerprints are termed as calibration data/calibration readings. Localization requests are obtained in the online stage and fall under the category of unlabeled data. These are the readings obtained from users who are interested in the estimation of their locations.

Unsupervised Manifold Alignment (UMA) [10] is used to tackle the problem of feature matching between the collected readings and the available coordinate plan of the indoor environment. The non-bijective mapping functions transfer the information from the readings data set to the coordinates data set. UMA does not require any correspondence information between the data sets to align them in the common lower dimensional manifold. The local features are learned and the connection of local geometries are obtained to learn the mappings. The mappings then transfer the data points to a common lower dimensional (hyper)plane. The

closest match between the point pairs from both sets in the common manifold will help in estimating the locations. UMA is superior to another unsupervised technique [11] as indicated in [10] in a sense that the complexity incurred during local feature matching is greatly reduced as well as separate mappings are obtained for tight alignment.

Another task in indoor localization problem involves the estimation of radio coverage of the indoor area. The APs available in the indoor area are not accessible at all the locations. For example, for a large indoor area such as a university campus or an airport, the AP accessible at north side of the area may not be accessible at the south side. This poses a need to estimate radio coverage in an indoor environment, which helps to categorize services offered[1] over Wi-Fi networks. The estimated radio map can also be used to estimate new localization requests directly from the map by means of much simpler algorithms like nearest neighbor (NN) and k-nearest neighbors approaches.

1.3 Organization of the Thesis

Chapter 2 describes briefly different techniques and methodologies, related to our work, that have been used earlier for location sensing. The chapter broadly categorizes the techniques, which use full and partial fingerprinting map. The importance of Wi-Fi based location fingerprinting approach, which we used, as

---

[1]These services are based on signal strength and are categorized into high data rate services like VoIP, video calling, video streaming and low data rate services like text chatting, browsing.

compared to other techniques is also discussed. The chapter also briefly discusses the unsupervised manifold alignment technique, which we used in our indoor localization framework. It also describes the importance of radio map estimation.

Chapter 3 describes the proposed technique for indoor localization. The proposed methodology makes use of novel unsupervised manifold alignment algorithm, which with geometry perturbation greatly improves the localization accuracy. The unsupervised manifold alignment obtains the matchings between the data sets that have same underlying correlation pattern. The data sets used to obtain the matchings comprise of RSS readings and indoor plan coordinates. The chapter describes the collection of the readings, formulation of the problem and finally its solution to obtain the position estimates. It describes how geometry perturbation greatly improves the performance. The further enhancement in performance is achieved by clustering the RSS readings and coordinates data sets considered in manifold alignment problem.

The proposed work for estimating radio map of the indoor environment is presented in Chapter 4. It discusses the problem formulation and usage of the results, from proposed indoor localization framework, for radio map estimation. The proposed work makes use of very limited information (few calibration readings and few localization requests with location estimations) to estimate the complete radio map of the indoor environment. The collected data is treated as labeled data and is used in conjunction with the indoor plan coordinates, which are divided into labeled and unlabeled locations. The linear least-mean-squares estimator is then

employed to estimate RSS values at all the unlabeled positions. The performance achieved here is at the expense of small amount of information.

Finally, Chapter 5 concludes the work and briefs the future trend.

CHAPTER 2

LITERATURE REVIEW

In this chapter, an overview on the existing works and methodologies for location sensing is presented. The notations used throughout the thesis are depicted in the following table. These are illustrated here for clarity since these will be used to address specific variables in later parts of the thesis.

Table 2.1: Summary of used notations

Type of variable	Notation
Scalar	Italicized, lower-case (e.g. m)
Constant	Italicized, upper-case (e.g. N)
Matrix	Bold-face, upper-case (e.g. $\mathbf{V}$)
Vector	Bold-face, lower-case (e.g. $\mathbf{v}$)
Set	Upper-case calligraphic font (e.g. $\mathcal{X}$)
i^{th} member of a set $\mathcal{X}$ (vector case)	Bold-face, lower-case subscript ($\mathbf{x}_i$)
i^{th} member of a set $\mathcal{X}$ (scalar case)	lower-case subscript (e.g. x_i)
k^{th} dimension of ith member of a set $\mathcal{X}$	lower-case (e.g. $x_k^{(i)}$)

Localization, especially indoor, has been under extensive research a while ago. Despite the ability of the Global Positioning System (GPS) to provide enough accuracy for outdoor positioning, it cannot be used in indoor environments since it becomes difficult to cope with the technical challenges encountered due to com-

plexity of indoor radio propagation. The positioning using the RSS of WLAN infrastructure has gained much importance recently due to the reduced installation costs. Moreover, no changes in hardware are required since almost all the modern mobile devices are equipped with WiFi cards (IEEE 802.11 standard [12]). Instead of installing new Access Points (APs) in the indoor environment, existing APs can be used for localization. The indoor positioning using WLAN RSS has already been proven advantageous over the angle-of-arrival (AoA), time-of-arrival (ToA)/time-difference-of-arrival (TDoA) measurement based algorithms since the RSS readings can be obtained effortlessly. The usage of WLAN RSS for positioning has been stressed in [1,2] because of its simplicity.

Some works [13–16] make use of the sensors (gyroscope, compass, accelerometer and Wi-Fi adapter) present in the mobile devices. Due to the internal structure of indoor area (people taking escalators, elevators, stairs or moving on the floor), the readings obtained from these sensors have particular trend. These readings actually give the idea of particular sub area in the whole area where the user would be present. The further algorithmic development then helps to localize users. Following sections describe these works briefly.

2.1   RSS-based WLAN Location Sensing

The indoor positioning using WLAN RSS is broadly divided into two categories. One method makes use of radio propagation models and statistical modeling [17–19]. The other method deals with location fingerprinting [20–23]. The

former method is unreliable since radio propagation is unpredictable in indoor environment. The location fingerprinting also has some limitations, which are discussed in Section 2.2.

The indoor positioning using RSS fingerprinting has been widely used in recent works [5, 7, 21–24]. It is based on collecting RSS fingerprints of the indoor environment to construct the radio map. These RSS fingerprints are obtained form APs at specific positions known as reference points [21] or grid points [24]. The RSS fingerprints follow a unique pattern in spatial domain and thus are like human fingerprints. Indoor positioning based on location fingerprinting involves two phases, namely the offline phase and the online phase.

1. **Offline Phase**

   The radio or fingerprint map is obtained in the offline phase where RSS readings from concerned APs are collected at each reference point in the indoor area. Once the radio map is collected, it is stored in the database for future reference. The physical space is discretized into N positions with a certain fixed distance in between the positions. Fig. 2.1 shows the discretization of the physical area into N grid points. The presence of R APs is also shown ($R = 4$ in this example).

   The RSS readings are obtained separately from R APs at the ith location in an indoor area and are stacked into a vector, $\mathbf{c}_i$, which is represented as:

$$\mathbf{c}_i = \begin{bmatrix} c_1^{(i)} & c_2^{(i)} & \cdots & c_R^{(i)} \end{bmatrix}^T \tag{2.1}$$

11
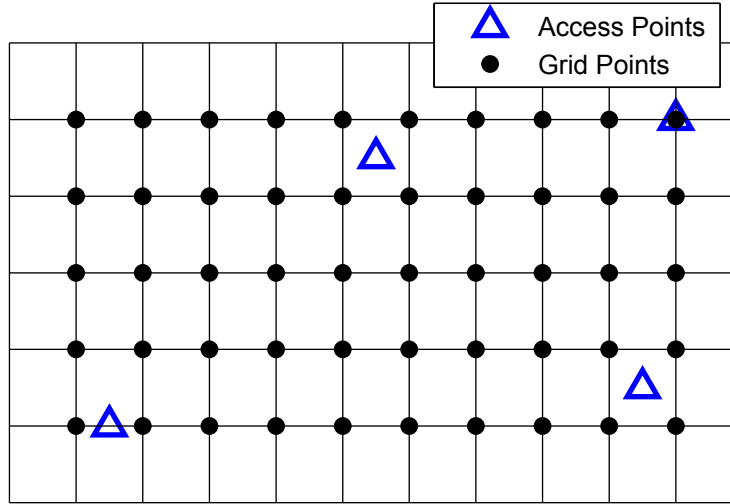
Figure 2.1: Discretization of Indoor Area. The number of APs shown here are 4

The radio or fingerprinting map is thus the collection of such vectors at all the N locations of the indoor environment and is represented as:

$$\mathcal{C} = \left\{ \begin{bmatrix} c_1^{(1)} \\ c_2^{(1)} \\ \vdots \\ c_R^{(1)} \end{bmatrix}, \begin{bmatrix} c_1^{(2)} \\ c_2^{(2)} \\ \vdots \\ c_R^{(2)} \end{bmatrix}, \cdots, \begin{bmatrix} c_1^{(N)} \\ c_2^{(N)} \\ \vdots \\ c_R^{(N)} \end{bmatrix} \right\} \tag{2.2}$$

As can be inferred from Fig. 2.1, the collection of fingerprints at all the locations of the indoor environment is quite hectic and time consuming process especially for enormous indoor areas (e.g. giant shopping malls, airports and hospitals) and/or of high dynamics (e.g. moving carts, persons and elevators in malls, moving trains in subway stations). The dynamic nature of an indoor environment poses the need for updating this database

after some time. This acts as the main hurdle in practical deployment of RSS based indoor localization systems.

2. **Online Phase**

   The online phase involves the collection of localization request(s) (RSS readings measured by user(s)). The localization algorithm is then run with the available information to estimate the position(s) of these users. The localization algorithms usually make comparison of the online measurements with the stored radio map.

2.2   Limitations of RSS Fingerprinting

The received signal strength (signal power) from a transmitter (Wi-Fi AP) falls inversely with the square of the distance from it in free space. However, in real environments, this is not the scenario. The building structure together with the moving objects inside it act as the major source of signal strength variations. These variations also change from one building structure to another. The cause of these effects can be broadly classified into large scale fading (shadowing) and small scale fading (multi-path) [25].

The large scale propagation effects cause spatial variations in RSS values. Taking care of these effects is really difficult. The path loss models should take care of antennas and device orientations. The antennas are normally anisotropic, which means that the power radiated/received from/to an antenna does not follow circular contours instead different power values are observed at different orientations

of the mobile device. The presence of human bodies in between the path of the wave makes the modeling of path loss more complex.

The small scale propagation effects occur due to multi-path and cause temporal variations in RSS values. The dynamics of the indoor environment such as moving people and objects act as the source of variation in RSS values. The RSS values in this case varies over the distance, which is in the order of the signal wavelength. The wavelength in case of WLANs is $\lambda = 0.125m$ for 2.4 GHz operational frequency, which decreases with higher operational frequency of 5 GHz.

The above mentioned effects make the modeling of RSS-distance relationship difficult in real indoor environments. So, the fingerprinting approach overcomes the spatial and temporal variations of RSS values to much extent. The spatial variations are modeled by collecting these values on a specified grid in an indoor environment. The accuracy increases by increasing the number of grid points[1]. The temporal variations are characterized by collecting large number of time samples of these values at a grid point.

2.3   Indoor Localization Schemes in Literature

Different approaches have been undertaken for location estimation by employing full or partial fingerprinting map. These are described as follows.

---

[1]The increase in number of grid points decrease the distance between them for the given indoor environment. The decreased distance results in grid of finer resolution, however, it increases the computational complexity.

14

2.3.1 Indoor Localization using Full Radio Map

The following schemes employ the complete radio map of the indoor environment.

The simplest solution for localization using the radio map is to find the centroid of the K nearest neighbors to the RSS reading of the localization request [6]. In this case, the distance of the localization request obtained in the online stage is computed with all the collected readings in the fingerprint database. The average of the database grid points having the K smallest RSS distances to the localization request is then taken and the coordinate is assigned to this localization request and sent to its user.

Another solution proposed in [21,23] makes use of compressive sensing [26–28]. These works treat the problem as sparse i.e. the users are sparse in the spatial domain and compressive sensing is employed for location estimation. The whole problem is divided into two stages, namely the coarse localization stage and the fine localization stage. In the coarse localization stage, all the fingerprints stored in the database are clustered by using Affinity Propagation [29]. In the online phase, the best matched clusters to a localization request are obtained by comparing the RSS reading of this request with the obtained cluster heads. The problem then shrinks to a smaller one which contains the subset of fingerprints inside these best matched clusters instead of the whole radio map. In fine localization stage, compressive sensing is employed where a sparse location vector is reconstructed by solving an l_1-norm minimization problem. The effect of device orientation is also taken into account in [22,23].

The problem is also treated as sparse in [24], in which the fingerprint map is constructed by taking into account the cross-correlation information of the signals at different APs. The locations of the users are reconstructed by solving an l_1-norm minimization problem. The cross-correlation information helps in the localization of large numbers of users with the same number of APs. Sometimes the problem becomes overdetermined, which can be solved by ordinary least squares. A similar solution methodology is proposed in [30] using TDoA and compressed sensing [26–28]. The cooperation among APs is taken into account to exploit the cross-correlation of signals at different APs. The fingerprinting map is constructed by making TDoA measurements on grid points throughout the indoor area. For localization, the online TDoA measurements are compared with the stored radio map. However, this TDoA solution is a passive localization technique, in which the location of the mobile user is estimated without its active involvement. The main drawback here is that extra hardware is needed for making signal measurements. Consequently, the WLAN location sensing using RSS fingerprints is more favorable since no investment is required in major equipment deployment for such systems and no hardware changes are required in the mobile devices.

2.3.2   Indoor localization using Partial Radio Map

To reduce the need, cost and effort in constructing and updating full radio maps, which is a must for all the solutions described in the previous section, another set of solutions are employing learning methods to either estimate the radio map or

localize using limited number of fingerprints.

One solution [8] makes use of limited number of fingerprints to estimate the positions. Almost 200 samples of RSS readings are accumulated at each calibration location. Total 137 grid points are considered for the indoor environment. The spacing between the points is not fixed but on average one grid point covers 19.5 m^2 of the area. The interpolation function is used which gives the (x,y) coordinates as the function of RSS values. The rms error is calculated for the location estimations. The work basically describes the effect on rms error by reducing the samples collected at a calibration position as well as lowering the number of calibration positions. The rms error reported is 9.19 m at 10 % of the total calibration load considered initially (i.e. 14 grid points out of 137). The best value of the rms error obtained is 3.75 m at 100 % of the total calibration load (i.e. 137 points).

Another recent example employed semi-supervised manifold alignment (SMA) [9] to solve the localization problem in the presence of limited number of fingerprints [5, 7]. In semi-supervised localization approaches, a small percentage of the RSS fingerprints is obtained throughout the indoor area and are termed as labeled data (calibration information/data/readings). The RSS readings from users are obtained in the online stage for location estimation and are called unlabeled data (localization requests). The SMA then aligns the labeled and unlabeled data in a common lower dimensional space. The data sets to be aligned are assumed to have (1) stronger correlation with the neighboring points as compared to dis-

tant points and (2) common lower dimensional correlation. The semi-supervised manifold alignment consists of the following main steps:

1. Weight computation by Locally Linear Embedding (LLE) [31]

   For the elements $\mathbf{x}_i$ and $\mathbf{x}_j$ in the data set $\mathcal{X}$, the LLE computes weight by

   $$\min_{W_{ij} \forall \mathbf{x}_j \in \mathcal{N}(\mathbf{x}_i)} \left| \mathbf{x}_i - \sum_{\mathbf{x}_j \in \mathcal{N}(\mathbf{x}_i)} W_{ij}\mathbf{x}_j \right|^2 \quad s.t. \sum_{\mathbf{x}_j \in \mathcal{N}(\mathbf{x}_i)} W_{ij} = 1 \qquad (2.3)$$

   where $\mathcal{N}(\mathbf{x}_i)$ is the set containing k nearest neighbors of $\mathbf{x}_i$. $W_{ij} = 0 \, \forall \mathbf{x}_j \notin \mathcal{N}(\mathbf{x}_i)$. The closest the point $\mathbf{x}_j$ to $\mathbf{x}_i$ the higher the weight assigned. The main advantage of using LLE is that it preserves the neighborhood correlation between the points.

2. Eigenvalue decomposition of the combined Laplacian matrix

After computing the weights, a combined Laplacian matrix [9] is constructed which consists of labeled elements from both the data sets, unlabeled elements from the first dataset and unlabeled elements from the second data set. The data sets are formed with labeled elements (denoted by subscript l) at the top followed by unlabeled elements (denoted by subscript u). Suppose we have data sets $\mathcal{X}$ and $\mathcal{Y}$. Considering Laplacian matrices $\mathbf{L}^{\mathcal{X}}$ and $\mathbf{L}^{\mathcal{Y}}$ for sets $\mathcal{X}$ and $\mathcal{Y}$ respectively, the combined Laplacian matrix $\mathbf{L}^{\mathcal{Z}}$ is of the form

$$\mathbf{L}^{\mathcal{Z}} = \begin{bmatrix} \lambda_x\mathbf{L}_{ll}^{\mathcal{X}} + \lambda_y\mathbf{L}_{ll}^{\mathcal{Y}} & \lambda_x\mathbf{L}_{lu}^{\mathcal{X}} & \lambda_y\mathbf{L}_{lu}^{\mathcal{Y}} \\ \\ \lambda_x\mathbf{L}_{ul}^{\mathcal{X}} & \lambda_x\mathbf{L}_{uu}^{\mathcal{X}} & \mathbf{0} \\ \\ \lambda_y\mathbf{L}_{ul}^{\mathcal{Y}} & \mathbf{0} & \lambda_y\mathbf{L}_{uu}^{\mathcal{Y}} \end{bmatrix} \qquad (2.4)$$

where λ_x and λ_y are the weighting factors defined in [7]. After eigenvalue decomposition of the combined Laplacian matrix, $\mathbf{L}^{\mathcal{Z}}$, the minimum d nonzero eigenvectors are obtained for d-dimensional embedding. The distances of the localization requests in this embedding domain are computed with all the remaining embedding and coordinates of the closest match are assigned to them. The algorithm shows good performance even when localization requests are increased. Nonetheless, the good performance is achieved at considerable percentage $(15 - 30\%)$ of fingerprints and thus more studies are required to further reduce these percentages while achieving similar performances.

2.3.3   Indoor Localization using Inertial Measurements

The following schemes make use of the data obtained from the sensors (such as gyroscope, compass, accelerometer) present in the mobile phones.

For instance, in [13], the location estimation is done using unsupervised approach, where the calibration effort is taken care of by the people roaming inside the area. The inertial sensors (such as accelerometer, gyroscope, compass and WNIC) present in the smart phones provide measurements that aid in localization. The readings obtained from these sensors are unique in the Wi-Fi space, that is, when a user walks, uses an escalator or an elevator, a particular effect is

observed on the readings obtained from these sensors. This information helps to point out the particular locations in an indoor area, which are called landmarks. The information is gathered from the people who walk randomly in the indoor area thus reporting their readings. The database is then formed using the readings obtained from the people. In the start, the algorithm shows poor performance but as the time passes, the algorithm converges to show good performance. This is because the data gathered from the people in the start of the deployment process helps to improve the location estimates thereafter. The reported accuracy of the system is around $2\ m$ but at the expense of gathering information from the indoor environment with the passage of time. So this seems to be the main hurdle in the practical deployment of such systems at large scales since the system needs to adapt itself to the new indoor environment.

The work in [16] deals with the generation of pathways in the indoor area. The data, here again, is gathered from the inertial sensors present in mobile phones. They also make use of the identified landmarks in the indoor area, which are obtained from the readings reported by users walking in the indoor area. The reported error is around $3\ m$. The accuracy obtained here is at the expense of running the algorithm for some time in the indoor area. The initial running of the algorithm actually helps to gather the crowd sourcing information. The initial adaptation of the algorithm to the area does not make it robust to changing indoors structures as well as deployment in the new area since some amount of time is required to obtain this level of accuracy.

The work in [15] also makes use of the RSS readings obtained from users as well as the sensory measurements in their smart phones. The RSS fingerprints are collected from the users walking in the indoor area. Based on the collected fingerprints, the overlapped fingerprints are merged. The stress-free floor plan and stress-free fingerprint space are constructed from the coordinate plan and the collected fingerprints respectively. The mapping between the spaces then help to estimate the users' locations. For practical deployment of the system, the users walk in the indoor area and send their accelerometer readings as wells as the collected RSS readings during the movement. The accelerometer readings help in estimating the distance covered by the user. The distance considered between the grid points is $2\ m$. The average localization error reported therein is $5.88\ m$. This is again at the expense of gathering information in the indoor environment initially.

The technique discussed in [14] also takes information from the inertial sensors (accelerometer, compass and gyroscope) present in smart phones. The information from these sensors help to estimate the motion of user. The collected readings from sensors as well as Wi-Fi adapter then help to estimate the locations. This work also requires much effort since users need to roam in the indoor area for some time to collect these readings. The algorithm developed is supposed to run in the background of the mobile phone. This puts some limitations on the practical implementation of the system since the processes running continuously in the background of the mobile phone will drain out its battery quickly.

The analysis of these techniques shows that still some time and resources are required for the practical deployment of such systems to obtain the acceptable level of localization accuracy. The above mentioned works need to collect information from the inertial sensors present in smart phones, which, in fact, adds to the additional hardware requirements. For each new indoor area, some sort of training procedure is required, which is a bottleneck in practical implementation of such systems.

2.4 Introduction to Unsupervised Manifold Alignment

Unsupervised Manifold Alignment [10, 11] (UMA) is currently used in many applications in machine learning (e.g. script matching between different languages, protein manifold alignment, image matching, pose matching between different types of image sets). Unlike semi-supervised manifold alignment, unsupervised manifold alignment does not require any correspondence information between the data sets i.e. no labeling information is required. The essential step is to estimate the similarities in local structures between the data sets without destroying local features within the data sets.

Wang and Mahadevan proposed in [11] an unsupervised manifold alignment algorithm, in which mapping functions α and β were computed for the two data sets. These functions transform the elements of the two data sets to a common

lower dimensional space by preserving the local features and matching the local geometries simultaneously. Since the elements then reside in the common space, so the comparison between the matching elements becomes easy. The major drawback in Wang's method is that the computational complexity is very high while matching the local geometries. Assuming k neighbors per point, $k!$ geometry permutations should be tested for every point. Another drawback is that the mapping functions obtained provide holistic alignment i.e. the mapping function obtained for a set is same for all the points in that set. This causes most of the points to map to the same locations in a lower dimensional manifold. The points cannot be distinguished from one another. This results in making many false matches.

The drawbacks in Wang's methods are taken care of in [10], where the complexity incurred during the matching of local features between the data sets is greatly reduced. This reduction is done by representing the neighbor information for the element in a set by B-spline curves [32]. The local feature matching information between the data sets is obtained by computing enveloped areas between these curves. Then, the mappings are obtained by non-holistic alignment as opposed to Wang's method i.e. the separate mappings α_i's are obtained for the concerned elements in the source set. These separate mappings help in achieving tight manifold alignment.

2.5   Significance of Radio Map Estimation

The WLAN coverage estimation in an indoor environment finds many useful applications. The estimation of signal strength from an AP in an indoor environment gives an idea of possible coverage throughout the region from that AP. The estimated signal strength values help to predict performance for using different services. For instance, VoIP services, video calling, video streaming require high data rates, which corresponds to good signal strength. For low data rate services like online browsing, text chatting, low signal strength values are also acceptable. Moreover, it also helps to find replacement locations for APs in an indoor environment for good radio coverage. The placement of a new AP can be judged based on the already available radio map. The new placement of APs can also help to reduce the spillage of the signals outside the indoor premises. At some regions in an indoor environment, same signal strength is observed from multiple APs. If an AP goes down for some reason then another AP can be used to provide coverage in that area.

2.6   Chapter Summary

This chapter describes the reason for opting RSS fingerprinting approach and its dominance over other methods, which is obviously because of its simplicity. However, there still exists the limitation of using RSS fingerprinting approach. The earlier work done on the subject is categorized into techniques, which employ full or partial fingerprinting map. This allows us to compare the performance of

our proposed approach, which greatly reduces the workload required by previous techniques. The unsupervised manifold alignment is also introduced briefly to give the reader an idea of how it can be used to obtain the mapping from the readings domain to the coordinates domain.

CHAPTER 3

PROPOSED INDOOR

LOCALIZATION

FRAMEWORK

This chapter describes the research methodology undertaken for indoor localization problem. A novel Unsupervised Manifold Alignment (UMA) algorithm [10] (described later in this chapter) with geometry perturbation is used to obtain the location estimates for localization requests. The source and destination data sets are required by UMA. The matching between the data sets then help to localize user(s). The following section describes the formulation of the indoor localization problem. This is followed by the explanation of geometry perturbation, unsupervised manifold alignment and the steps describing localization algorithm. Finally, the clustering is introduced to further improve the performance.

3.1 Problem Formulation

As described in the previous chapter, RSS fingerprints (from now on, for simplicity, the term "fingerprints" will be used to indicate "RSS fingerprints" wherever required) are used for location sensing. To build the problem, some RSS readings are collected. These include few calibration readings (another name used for fingerprints), some crowd sourced readings (RSS readings gathered from casual users walking in the indoor area), localization request(s) (RSS readings measured by user(s) to obtain their location(s)) and indoor plan coordinates. The main point to note here is that very small number of fingerprints (approximately 1% of all grid points in the indoor area, that is, 2 points in our case) are used in this work. The collected RSS readings (calibration readings, crowd sourced readings and localization requests) and plan coordinates of the indoor area are arranged in the form of source and destination data sets. The unsupervised manifold alignment with geometry perturbation then aligns the data sets in a common lower dimensional (hyper)plane.

As mentioned in Section 2.1, the indoor area is discretized into N grid points or positions with some fixed distance in-between the points. The fingerprints are obtained at these points (in our case as low as 1% of the total grid points in the indoor area). The calibration readings or fingerprints are obtained in the offline stage and crowd sourced readings and localization requests in the online stage. Since very small number of fingerprints (1% i.e. 2 in our experiments) are used for location estimations so these fingerprints can also be collected in

the online stage by use of sniffers, which are hardware or computer programs that log or intercept traffic over wireless or Ethernet Local Area Network (LAN). This eliminates the workload completely, that is, the database of these very few fingerprints can be updated continuously without the aid of manpower. Following subsections describe the construction of source and destination data sets.

3.1.1 Source Data Set

The source data set $\mathcal{X}$ contains R-dimensional vectors representing the RSS readings measured from R APs. The set $\mathcal{X}$ is constructed by concatenating the fingerprints or calibration readings set $\mathcal{C}$, the crowd sourced readings set $\mathcal{O}$ and the localization requests set $\mathcal{L}$. Note that the calibration readings are readings obtained at known locations whereas crowd sourced readings are received from unknown locations. Consider the calibration readings set $\mathcal{C}$. Each element $\mathbf{c}_i$ of $\mathcal{C}$ is a vector of RSS measurements obtained at a known position i in the spatial domain from R APs. In other words:

$$\mathbf{c}_i = \left[\begin{array}{cccc} c_1^{(i)} & c_2^{(i)} & \cdots & c_R^{(i)} \end{array} \right]^T \tag{3.1}$$

We can thus describe $\mathcal{C}$ as:

$$\mathcal{C} = \left\{ \begin{bmatrix} c_1^{(1)} \\ c_2^{(1)} \\ \vdots \\ c_R^{(1)} \end{bmatrix}, \begin{bmatrix} c_1^{(2)} \\ c_2^{(2)} \\ \vdots \\ c_R^{(2)} \end{bmatrix}, \cdots, \begin{bmatrix} c_1^{(f)} \\ c_2^{(f)} \\ \vdots \\ c_R^{(f)} \end{bmatrix} \right\} \tag{3.2}$$

These fingerprints are obtained at f grid points, which, as indicated earlier, are very small in number as compared to the total grid points of the indoor area under consideration (that is, $f \ll N$). Similarly, the elements present in crowd sourced readings set $\mathcal{O}$ and the localization requests set $\mathcal{L}$ also contain RSS readings, in vector form, from R APs. The ith element of these sets are given by, respectively,

$$\mathbf{o}_i = \begin{bmatrix} o_1^{(i)} & o_2^{(i)} & \cdots & o_R^{(i)} \end{bmatrix}^T \tag{3.3}$$

$$\mathbf{l}_i = \begin{bmatrix} l_1^{(i)} & l_2^{(i)} & \cdots & l_R^{(i)} \end{bmatrix}^T \tag{3.4}$$

Thus, the sets $\mathcal{O}$ and $\mathcal{L}$ are described by:

$$\mathcal{O} = \left\{ \begin{bmatrix} o_1^{(1)} \\ o_2^{(1)} \\ \vdots \\ o_R^{(1)} \end{bmatrix}, \begin{bmatrix} o_1^{(2)} \\ o_2^{(2)} \\ \vdots \\ o_R^{(2)} \end{bmatrix}, \cdots, \begin{bmatrix} o_1^{(s)} \\ o_2^{(s)} \\ \vdots \\ o_R^{(s)} \end{bmatrix} \right\} \tag{3.5}$$

29

$$
\begin{array}{cccc}
c_1^{(1)} & c_2^{(1)} & \cdots & c_R^{(1)} \\
c_1^{(2)} & c_2^{(2)} & \cdots & c_R^{(2)} \\
& & \vdots & \\
c_1^{(f)} & c_2^{(k)} & \cdots & c_R^{(f)} \\
o_1^{(1)} & o_2^{(1)} & \cdots & o_R^{(1)} \\
o_1^{(2)} & o_2^{(2)} & \cdots & o_R^{(2)} \\
& & \vdots & \\
o_1^{(s)} & o_2^{(s)} & \cdots & o_R^{(s)} \\
l_1^{(1)} & l_2^{(1)} & \cdots & l_R^{(1)} \\
l_1^{(2)} & l_2^{(2)} & \cdots & l_R^{(2)} \\
& & \vdots & \\
l_1^{(r)} & l_2^{(r)} & \cdots & l_R^{(r)}
\end{array}
$$

Figure 3.1: Structure of Readings Data Set $\mathcal{X}$

$$
\mathcal{L} = \left\{ \begin{bmatrix} l_1^{(1)} \\ l_2^{(1)} \\ \vdots \\ l_R^{(1)} \end{bmatrix}, \begin{bmatrix} l_1^{(2)} \\ l_2^{(2)} \\ \vdots \\ l_R^{(2)} \end{bmatrix}, \cdots, \begin{bmatrix} l_1^{(r)} \\ l_2^{(r)} \\ \vdots \\ l_R^{(r)} \end{bmatrix} \right\} \tag{3.6}
$$

The structure of the source data set $\mathcal{X}$ is:

$$
\mathcal{X} = \{ \mathbf{c}_1, \cdots, \mathbf{c}_f, \mathbf{o}_1, \cdots, \mathbf{o}_s, \mathbf{l}_1, \cdots, \mathbf{l}_r \} \tag{3.7}
$$

The total number of elements in set $\mathcal{X}$ is $M = f + s + r$, which is the cardinality of this set. Figure 3.1 shows the pictorial view of this arrangement. As stated earlier, the set $\mathcal{X}$ is comprised of three portions. The first portion of the set $\mathcal{X}$, which represents the calibration readings or fingerprints, is not used in unsupervised manifold alignment but rather in perturbing the local geometries of the indoor

30
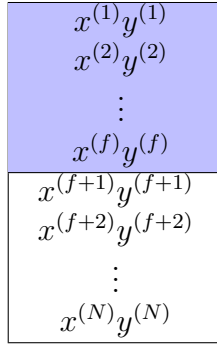
Figure 3.2: Structure of Coordinates Data Set $\mathcal{Z}$

plan coordinates. This will become clear in the upcoming sections.

3.1.2 Destination Data Set

The destination data set $\mathcal{Z}$ is formed using 2-dimensional coordinates correspond-
ing to the physical locations in the indoor area. These elements are arranged in
such a manner that the first f coordinate pairs are in correspondence with the cal-
ibration readings and remaining portion of the set contains remaining coordinates
of the indoor area. This set is represented as:

$$\mathcal{Z} = \{\mathbf{p}_1, \cdots, \mathbf{p}_f, \mathbf{p}_{f+1}, \cdots, \mathbf{p}_N\} \tag{3.8}$$

where, the ith element represents the ith coordinate pair and is given as:

$$\mathbf{p}_i = \begin{bmatrix} x^{(i)} \\ y^{(i)} \end{bmatrix} \tag{3.9}$$

Figure 3.2 shows the pictorial view of the coordinates data set $\mathcal{Z}$. The cardinality
of the set $\mathcal{Z}$ is N. The main point to note here is that $M \neq N$, which necessarily

implies that $(s + r) \neq (N - f)$. Since the RSS readings are taken at some coordinates so M is usually much less than N. The output of the algorithm provides estimated positions of the last r readings or localization requests in the set $\mathcal{X}$. That is,

$$\hat{\mathcal{P}}_{\mathcal{L}} = \{\hat{\mathbf{p}}_{l_1}, \hat{\mathbf{p}}_{l_2}, \cdots, \hat{\mathbf{p}}_{l_r}\} \tag{3.10}$$

These estimated positions with associated RSS readings help in estimating the radio map in the indoor area. This is described later in the thesis.

3.2 Unsupervised Manifold Alignment

Unlike its semi-supervised counterpart [9], unsupervised manifold alignment [10] is a transfer learning technique that does not need any correspondence information to align the data sets in a lower dimensional space. It replaces the considerable percentage of labeled data (in our case fingerprinted RSSs) required for the semi-supervised approach by unlabeled data (in our case crowd sourced RSSs). To perform manifold alignment in such an unsupervised environment, the similar correlation patterns of the source and destination data sets (i.e. the fact that neighboring points have stronger correlation as compared to distant points) is exploited. This assumption allows the matching of intrinsic structures between the data sets. Instead of performing a transformation of the data sets to a common lower dimensional space, the source data set is transformed by a non-bijective mapping function to the destination data set. The perfect matchings are then obtained by comparison. Following points are important while aligning the data

sets in a common lower dimensional space.

1. Preservation of local geometries within the data sets.

2. Matching of local geometries between the data sets.

Consider our two sets, the source set $\mathcal{X}$ with M elements:

$$\mathcal{X} = \{\mathbf{x}_1, \mathbf{x}_2, \cdots, \mathbf{x}_M\} \tag{3.11}$$

and the destination set $\mathcal{Z}$ with N elements:

$$\mathcal{Z} = \{\mathbf{z}_1, \mathbf{z}_2, \cdots, \mathbf{z}_N\} \tag{3.12}$$

The perfect geometry matchings are obtained between these data sets by simultaneously preserving the local geometries. The following subsections describe these points of aligning data for this specific application.

3.2.1   Geometry Perturbation of Destination Data Set

As stated earlier, the plan coordinates are used as destination data set in manifold alignment problem. The important point in manifold alignment is the matching of local geometries between both the sets, so these local geometries must be different and hopefully unique for each locality of the data set. Since the plan coordinates usually follow a regular pattern (i.e. they are usually represented by a grid structure with equal spacing between coordinate points) consequently, it becomes hard

to differentiate small chunk of coordinates from one place to another in an indoor area. Consider again the example of an indoor area shown in Figure 2.1. Figure 3.3 shows the scenario of regular geometry of plan coordinates. To resolve this issue and create uniqueness throughout the coordinate plan local geometries, the use of very small number of fingerprinted readings (as low as 1%, i.e. 2 points in our case) is proposed to create a perturbation in such geometries. In other words, the fingerprinted data is responsible only for introducing such uniqueness throughout the coordinate plan localities. Figure 3.4 shows the idea of geometry perturbation. By comparing Figures 3.3 and 3.4, it can be inferred that each grid point can be represented uniquely in the spatial domain. The bold red dots in Figure 3.4 represent the fingerprinted data. These points act as neighbors for all other points in the indoor area. If geometry perturbation is not taken into ac-
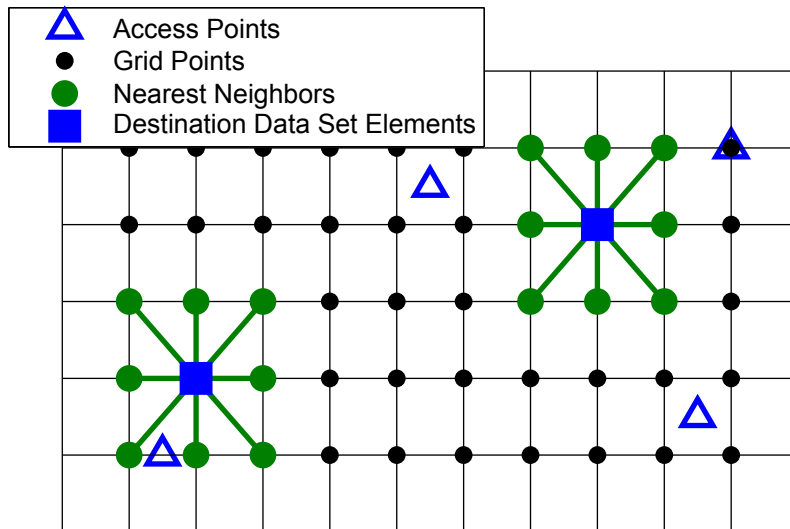
Figure 3.3: Regular geometry of the indoor plan coordinates

count, then many false matches will occur, which results in high localization errors as will be illustrated in experimental results shown later. This is assumed that
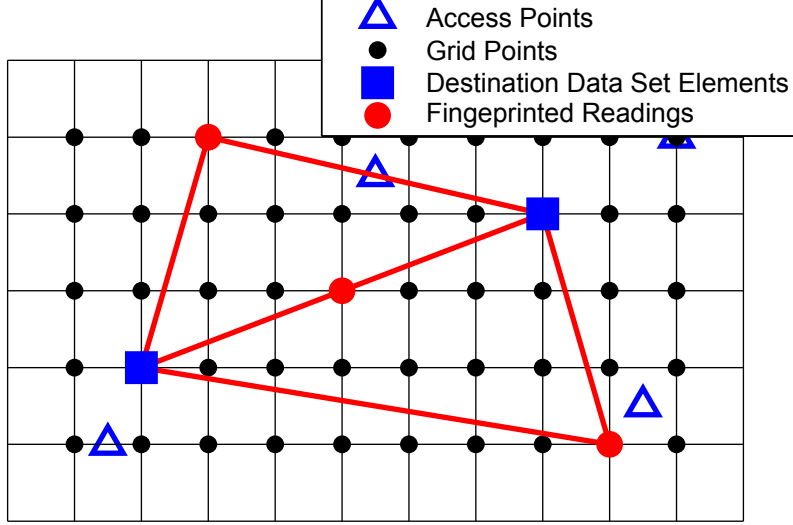
Figure 3.4: Perturbed geometry of the indoor plan coordinates

this fingerprinted data (RSSs and their coordinates) is introduced as first f data points in both the data sets. The remaining readings in set $\mathcal{X}$ consist of crowd sourced information and localization requests and the remaining elements in set $\mathcal{Z}$ are the remaining coordinates of the indoor plan. Let $\mathcal{X}_r$ and $\mathcal{Z}_r$ represent the remaining elements in sets $\mathcal{X}$ and $\mathcal{Z}$ respectively. These are given as:

$$\mathcal{X}_r = \{\mathbf{x}_{f+1}, \mathbf{x}_{f+2}, \cdots, \mathbf{x}_M\} \tag{3.13}$$

$$\mathcal{Z}_r = \{\mathbf{z}_{f+1}, \mathbf{z}_{f+2}, \cdots, \mathbf{z}_N\} \tag{3.14}$$

To create the necessary geometry perturbation required for correct matching of geometries, the first f calibration elements are used as neighbors for all the other elements in the respective sets and discrete distance vectors are obtained. For the

i^{th} element in set $\mathcal{X}_r$, the discrete distance vector is as follows:

$$\mathbf{e}_i^{\mathcal{X}_r} = \begin{bmatrix} 0 & e_{i1} & \cdots & e_{if} \end{bmatrix}^T, \quad i = 1, 2, \cdots, M - f \qquad (3.15)$$

where, the first entry represents the distance of the ith element with itself, which is equal to 0, and the remaining entries represent the distance with the first f elements in set $\mathcal{X}$. Similarly, the discrete distance vectors are obtained for all the elements in set $\mathcal{Z}_r$, which for the jth element in this set, can be represented as:

$$\mathbf{e}_j^{\mathcal{Z}_r} = \begin{bmatrix} 0 & e_{j1} & \cdots & e_{jf} \end{bmatrix}^T, \quad j = 1, 2, \cdots, N - f \qquad (3.16)$$

3.2.2 Matching of Local Geometries

One very recent method to represent and match local geometries in unsupervised manifold alignment is the use of spline curves. These spline curves can be used to match local geometries as follows. The spline curves (which are continuous parameterized curves) are fitted to the distance vectors $\mathbf{e}_i^{\mathcal{X}_r}$ and $\mathbf{e}_j^{\mathcal{Z}_r}$, which are obtained as shown previously. So there are $(M - f)$ curves in the source data set $\mathcal{X}_r$ and $(N - f)$ curves in destination data set $\mathcal{Z}_r$. The number of curves in respective sets correspond to the cardinalities of these sets. The closeness of the local geometry of one element in the source data set with that of the other element in destination data set is measured by the enveloped area and gradient between the curves. Define $g_i^{\mathcal{X}_r}$ and $g_j^{\mathcal{Z}_r}$ as the curves fitted to the discrete distance vectors corresponding to the ith element in set $\mathcal{X}_r$ and j^{th} element in set $\mathcal{Z}_r$, respectively,

36

using cubic spline interpolation [32]. The curves defined by $g_i^{\mathcal{X}_r}$'s are normalized to 1. Similarly, the process is repeated for the curves defined by $g_j^{\mathcal{Z}_r}$'s. This is because the RSS readings are higher dimensional as compared to the coordinates. When the discrete distance vectors are obtained from the elements in the RSS readings set, the distance values are larger as compared to those obtained from the elements in the coordinates data set. Normalizing to 1 helps to obtain good closeness measure between the elements from these two sets. Also, define $\nabla g_i^{\mathcal{X}_r}$ and $\nabla g_j^{\mathcal{Z}_r}$ the gradients of $g_i^{\mathcal{X}_r}$ and $g_j^{\mathcal{Z}_r}$, respectively. We can thus define $\mathbf{H}$ as the local geometry similarity matrix, whose $i - j$'s element h_{ij} (referred to as local geometry similarity indicator) is given by:

$$h_{ij} = \int_0^f \left(\left| g_i^{\mathcal{X}_r} - g_j^{\mathcal{Z}_r} \right| + \beta \left| \nabla g_i^{\mathcal{X}_r} - \nabla g_j^{\mathcal{Z}_r} \right| \right) du \qquad (3.17)$$

where β is a balancing constant and u is the integration variable. The integration is solved by the Composite Simpson's rule [32]. This creates a matrix $\mathbf{H} = [h_{ij}]$ of size $(M - f) \times (N - f)$. Figure 3.5 shows the spline curves for the elements taken from the source and destination data sets. Now we can use the similarity indicator h_{ij} to find the best matching between $\mathcal{X}_r$ and $\mathcal{Z}_r$ and hence create the local geometry matching set $\mathcal{D}$ as the set of pairs as follows:

$$\mathcal{D} = \left\{ (\mathbf{x}_i, \mathbf{z}_j) \, | h_{ij} = \min_{1 \le t \le N - f} h_{it}, \text{ and } h_{ij} < \eta \right\} \qquad (3.18)$$
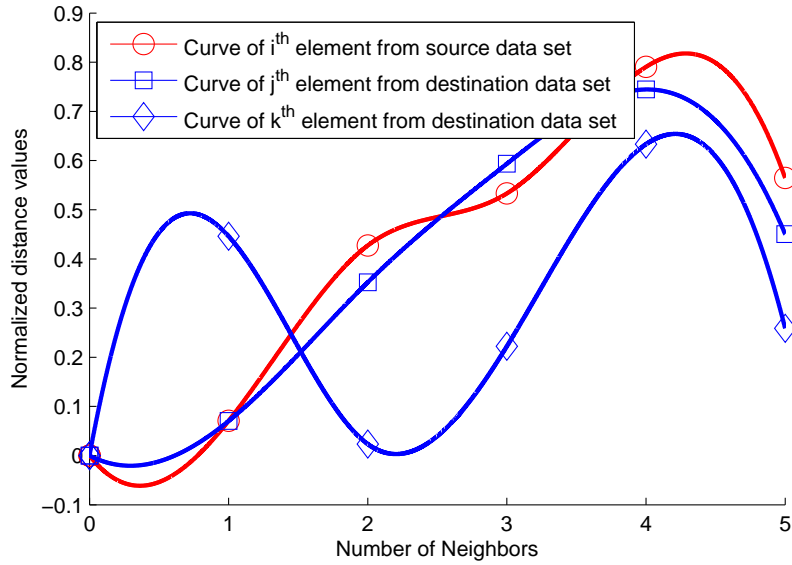
Figure 3.5: Cubic spline curves from the source and destination data sets, (a) the red curve is from the source data set, and (b) the blue curves are from the destination data set. The blue curve with square markers has higher similarity to the red curve as compared to the other one with diamond markers

In other words, the data point $\mathbf{z}_j$ from set $\mathcal{Z}_r$ is considered to be matched with point $\mathbf{x}_i$ from set $\mathcal{X}_r$, and thus are added as a matched pair $(\mathbf{x}_i, \mathbf{z}_j)$ to $\mathcal{D}$, if it has the largest similarity (i.e. smallest h_{ij}) among all other points in $\mathcal{Z}_r$ and h_{ij} is below a certain threshold η. In this matching set two points $\mathbf{x}_i$ and $\mathbf{x}_i'$ might be matched to the same coordinate $\mathbf{z}_j$ and that some $\mathbf{x}_i$'s might not get any matches.

3.2.3 Manifold Alignment

After obtaining some matched pairs in set $\mathcal{D}$, we have two types of elements in the source set $\mathcal{X}_r$, namely the ones that are matched to elements in destination set $\mathcal{Z}$ and the ones that are not. So we have to give high weight to these matched pairs in the alignment formulation as will be described shortly. The preservation

of local geometries is also essential while aligning data in a lower dimensional space. Taking these facts into account, the objective function for the unsupervised manifold alignment formulation consists of three terms J_d, J_f and J_s, which are responsible for minimizing the inter-manifold distance, local geometry matching between the data sets and preservation of local geometries within the data set, respectively.

Consider an affine transformation matrix $\boldsymbol{\alpha}_i$, which is assigned to the element $\mathbf{x}_i$ in $\mathcal{X}_r$. The matrix $\boldsymbol{\alpha}_i$ is of dimension $2 \times R$, where 2 is the dimension of the coordinates and R represents the number of access points, that is, the dimensionality of the element in the source (RSS readings) data set $\mathcal{X}$. The term J_d contains elements of the set $\mathcal{X}_r$, which are not present in the local geometry matching set $\mathcal{D}$ and is expressed as:

$$J_d = \sum_{\mathbf{x}_i \in \mathcal{X}_r,\, (\mathbf{x}_i, \mathbf{z}_j) \notin \mathcal{D}} \min_{\mathbf{z}_j \in \mathcal{Z}} \|\boldsymbol{\alpha}_i \mathbf{x}_i - \mathbf{z}_j\|_2^2 \tag{3.19}$$

Let $\mathbf{z}_j$ be the element in $\mathcal{Z}$ that gives the lowest inter-manifold distance for $\mathbf{x}_i$. Thus, we get:

$$J_d = \sum_{\mathbf{x}_i \in \mathcal{X}_r,\, (\mathbf{x}_i, \mathbf{z}_j) \notin \mathcal{D}} \left(\mathbf{x}_i^T \boldsymbol{\alpha}_i^T \boldsymbol{\alpha}_i \mathbf{x}_i - \mathbf{x}_i^T \boldsymbol{\alpha}_i^T \mathbf{z}_j - \mathbf{z}_j^T \boldsymbol{\alpha}_i \mathbf{x}_i + \mathbf{z}_j^T \mathbf{z}_j \right) \tag{3.20}$$

Let ∇J_d denotes the gradient of J_d. We thus get:

$$\nabla J_d = \sum_{\mathbf{x}_i \in \mathcal{X}_r,\, (\mathbf{x}_i, \mathbf{z}_j) \notin \mathcal{D}} \left(2\boldsymbol{\alpha}_i \mathbf{x}_i \mathbf{x}_i^T - 2\mathbf{z}_j \mathbf{x}_i^T \right) \tag{3.21}$$

The term J_f contains elements of set $\mathcal{X}_r$, which are present in the local geometry matching set $\mathcal{D}$ and is expressed as:

$$J_f = \sum_{(\mathbf{x}_i, \mathbf{z}_j) \in \mathcal{D}} \|\boldsymbol{\alpha}_i \mathbf{x}_i - \mathbf{z}_j\|_2^2 \, w_{ij} \tag{3.22}$$

where w_{ij} is the weight computed between $\mathbf{x}_i$ and $\mathbf{z}_j$ by heat kernel i.e. $w_{ij} = e^{-\frac{h_{ij}^2}{\gamma}}$. The choice of γ is described in the results section. Expanding the term as done previously, we get

$$J_f = \sum_{(\mathbf{x}_i, \mathbf{z}_j) \in \mathcal{D}} \left(\mathbf{x}_i^T \boldsymbol{\alpha}_i^T \boldsymbol{\alpha}_i \mathbf{x}_i - \mathbf{x}_i^T \boldsymbol{\alpha}_i^T \mathbf{z}_j - \mathbf{z}_j^T \boldsymbol{\alpha}_i \mathbf{x}_i + \mathbf{z}_j^T \mathbf{z}_j \right) w_{ij} \tag{3.23}$$

and its gradient is:

$$\nabla J_f = \sum_{(\mathbf{x}_i, \mathbf{z}_j) \in \mathcal{D}} \left(2\boldsymbol{\alpha}_i \mathbf{x}_i \mathbf{x}_i^T - 2\mathbf{z}_j \mathbf{x}_i^T \right) w_{ij} \tag{3.24}$$

For preservation of local geometries, neighboring information is taken into account. So the crowd sourced information together with the localization requests serve the purpose by getting k nearest neighbors (knn) among them for the point $\mathbf{x}_i$. The last term, J_s, is responsible for preservation of local geometries. This is expressed as:

$$J_s = \sum_{\mathbf{x}_i \in \mathcal{X}_r} \sum_{\mathbf{x}_j \in knn(\mathbf{x}_i)} \|\boldsymbol{\alpha}_i - \boldsymbol{\alpha}_j\|_F^2 \tag{3.25}$$

where $knn(\mathbf{x}_i)$ is the set of the k nearest neighbors of $\mathbf{x}_i$. Minimizing this term results in minimizing the distances of the mappings of the k nearest neighbors of

$\mathbf{x}_i$ to its own mapping. Expanding J_s yields

$$J_s = \sum_{\mathbf{x}_i \in \mathcal{X}_r} \sum_{\mathbf{x}_j \in knn(\mathbf{x}_i)} Tr \left(\boldsymbol{\alpha}_i \boldsymbol{\alpha}_i^T - \boldsymbol{\alpha}_i \boldsymbol{\alpha}_j^T - \boldsymbol{\alpha}_j \boldsymbol{\alpha}_i^T + \boldsymbol{\alpha}_j \boldsymbol{\alpha}_j^T \right) \tag{3.26}$$

and its gradient is:

$$\nabla J_s = \sum_{\mathbf{x}_i \in \mathcal{X}_r} \sum_{\mathbf{x}_j \in knn(\mathbf{x}_i)} (2\boldsymbol{\alpha}_i - 2\boldsymbol{\alpha}_j) \tag{3.27}$$

The overall objective function to be minimized is thus the combination of the aforementioned three terms, and is given as:

$$J = \mu_d J_d + \mu_f J_f + \mu_s J_s \tag{3.28}$$

and its gradient is represented as:

$$\nabla J = \mu_d \nabla J_d + \mu_f \nabla J_f + \mu_s \nabla J_s \tag{3.29}$$

where μ_d, μ_f and μ_s are weighting factors for their respective terms, which are chosen empirically. Here μ_f is given the largest weight to stress on the matching of local geometries and μ_d is given the least weight.

The Quasi-Newton BFGS algorithm [33] is employed to solve this nonlinear optimization problem. The objective function along with the gradients are supplied to the Quasi-Newton BFGS algorithm. The optimized values of mappings $\boldsymbol{\alpha}_i$'s are obtained. These mappings then transform the elements in the source data set to the destination data set. The best matchings are then obtained by a

mapping function, which computes the closest point pairs.

3.3 Localization Algorithm

In this section, the above tailored unsupervised manifold alignment algorithm is applied to localize users using approximately 1% calibration readings, some crowd sourced readings, localization requests and plan coordinates of the indoor area. The goal is to learn the mappings $\boldsymbol{\alpha}_i$'s described previously. The data sets follow the assumed correlation pattern (i.e. the neighboring points have stronger correlation as compared to distant points.). The localization algorithm consists of the following steps:

1. Build the source and destination data sets as defined in Equations (3.7) and (3.8) respectively.

2. Obtain the spline curve for each element in sets $\mathcal{X}$ and $\mathcal{Z}$ except for the first f elements as described in Section 3.2.

3. The local geometry similarity matrix $\mathbf{H}$ is obtained by using Equation (3.17).

4. The cost function is set up as described in Section 3.2.3 Equation (3.28) and then the Quasi-Newton BFGS algorithm is applied to obtain the optimized transformation matrices, $\boldsymbol{\alpha}_i$'s.

5. For localization requests (last r elements in set $\mathcal{X}$), the positions are esti-

mated by computing the mapping function $\phi(\mathbf{x}_i)$,

$$\phi(\mathbf{x}_i) = \arg\min_{\mathbf{z}_j \in \mathcal{Z}} \|\boldsymbol{\alpha}_i \mathbf{x}_i - \mathbf{z}_j\|_2 \qquad (3.30)$$

$\mathbf{z}_j$, for which $\phi(\mathbf{x}_i)$ is minimum, represents the closest match. This, in fact, is the estimated position, $\hat{\mathbf{p}}_{l_i}$ (see Equation (3.10)).

3.4   Testing Results

This section describes the testing of proposed scheme using the real measurements from the 4th floor of Bahen Center, at University of Toronto, depicted in Figure 3.6, which is the same indoor plan used in [5]. The black dots represent the 219 plan coordinates considered in this indoor environment. The distance between each two neighboring points is 1 m. This indoor environment is used for comparison of the results with the previously proposed semi-supervised solutions. The indoor area under consideration is shown in Figure 3.7 without the building layout and APs. This plan just shows the grid points. This figure will be used to explain the idea of clustering, which is described later in this chapter.

The data collection is done in the same way as described in [5, 7]. For testing the algorithm as scenario independent, the crowd sourced readings and localization requests are chosen randomly throughout the indoor environment. Only set $\mathcal{C}$ is obtained in the offline stage while rest of the readings (crowd sourced information and localization requests) are obtained in the online stage. The mean localization
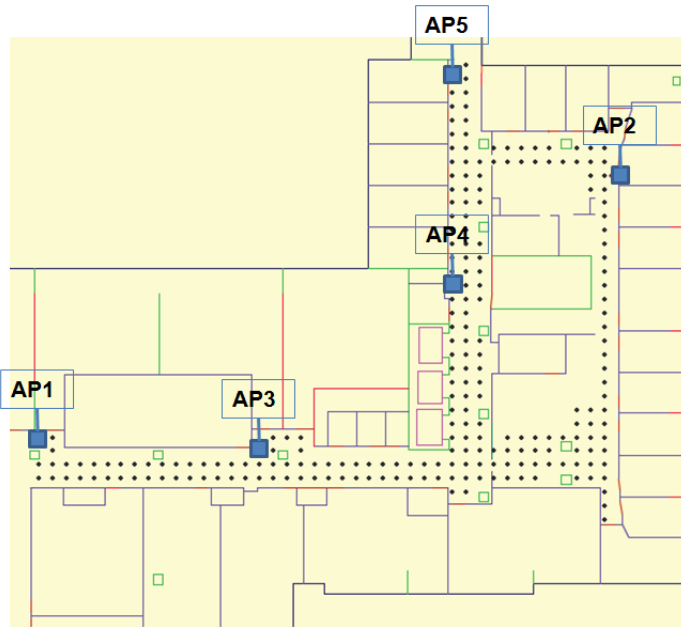
Figure 3.6: Floor plan of the indoor environment considered in testing
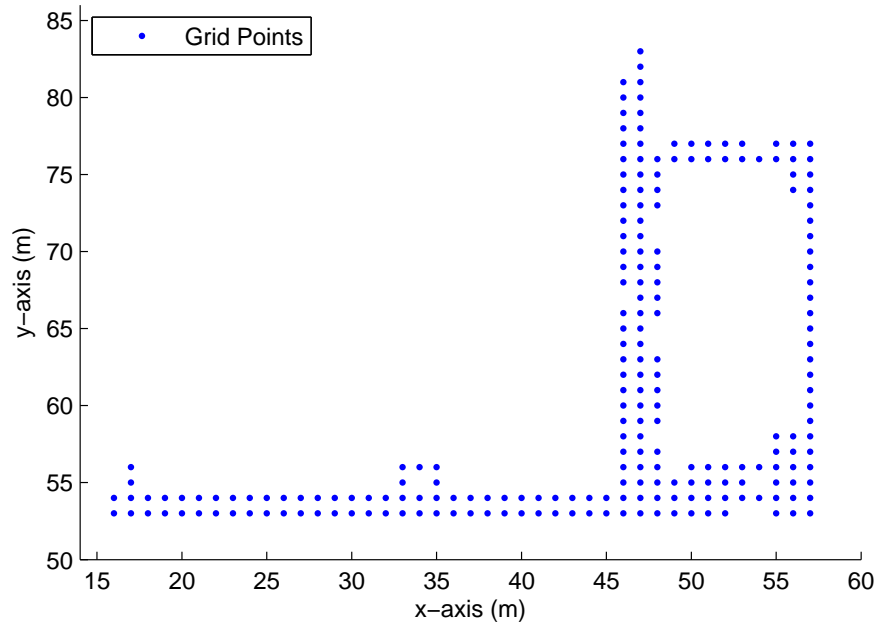
Figure 3.7: Floor plan of the considered indoor environment without building layout and APs

error (average error of all location estimations) is plotted against the variation of different parameters. The percentage variation shown for some parameters is

obtained by normalizing against the total number of points in the indoor area. The curves are obtained by averaging over a large number of runs of the algorithm. The chosen value of β is 0.1 for numerical integration and η is set at the lower 15% of the total values in matrix $\mathbf{H}$. The values of μ_d, μ_f and μ_s are set to 0.1, 10 and 1, respectively. The choice of γ (appearing in weight computation by heat kernel, $w_{ij} = e^{-\frac{h_{ij}^2}{\gamma}}$) is made by using $\gamma = -\frac{\eta^2}{\ln(0.9)}$, where η is described previously. The choice of γ makes all the values fall within 10% of the decay from maximum value as selected by η.

For comparisons while testing, following methodologies are considered:

- The proposed unsupervised manifold alignment algorithm with geometry perturbation.

- Unsupervised manifold alignment algorithm without geometry perturbation.

- The raw semi-supervised algorithm proposed in [5, 7] which considers the fingerprinted readings and localization requests only and excludes the crowd sourced information.

- A modified version of the semi-supervised algorithm in [5, 7], where the crowd sourced readings are treated as localization requests.

- The interpolation formulation, proposed in [8], makes use of radial basis functions. The estimated position is the function of RSS readings.

The following subsections show the effect of varying different parameters on the mean localization error.

3.4.1 Localization Errors of Individual Runs
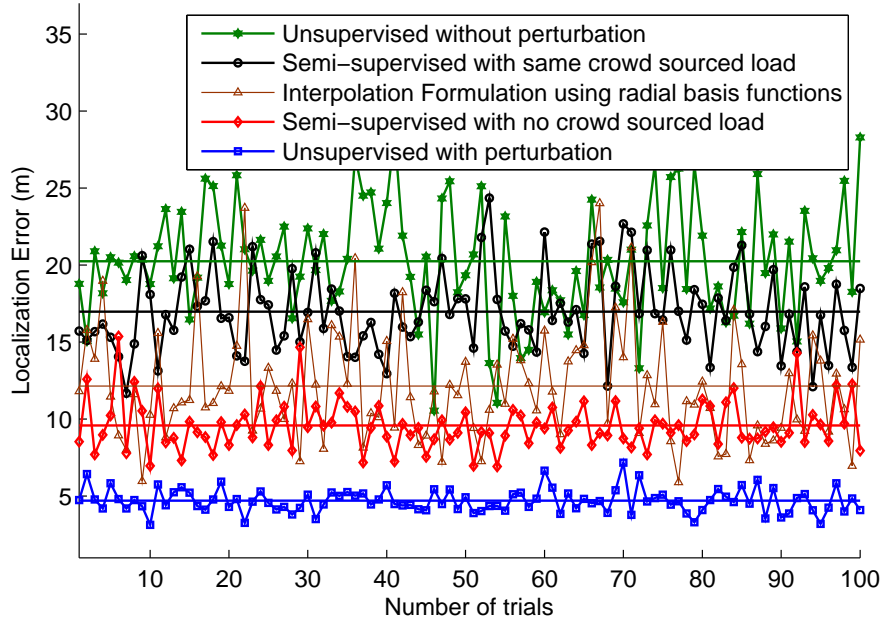
Figure 3.8: Localization error against the number of algorithm runs

Figure 3.8 depicts the localization error for individual runs of the methodologies described above for a fingerprinting load of approximately 1% (only 2 readings in our case). The crowd sourced readings are set to 10% and the localization requests are set to 7%. The figure clearly shows that the performance of the proposed unsupervised technique with a minimal calibration load for geometry perturbation is much better as compared to both variants of the semi-supervised approaches in terms of the mean and variance of the localization error. The results also show that the proposed geometry perturbation is a core point in achieving this huge improvement in performance compared to the raw unsupervised approach, thus proving the merits of the proposed algorithm. The performance is also better as compared to the interpolation formulation as described in [8].

Table 3.1: Comparison with respect to mean and variance

Algorithm	Mean (m)	Variance
Unsupervised without perturbation	20.24	13.45
Semi-supervised with same crowd sourced load	16.98	7.04
Interpolation Formulation using radial basis functions	12.14	13.69
Semi-supervised with no crowd sourced load	9.58	2.53
Unsupervised with perturbation	4.7	0.58

Table 3.1 summarizes the numerical comparison of the mean and variance of the reported error trends in Figure 3.8. Clearly, our proposed scheme with geometry perturbation significantly outperforms all other schemes at this very low level of fingerprinting load, both in the mean and variance of the localization error.

3.4.2 Variation of Calibration Readings (Fingerprinting Load)

Figure 3.9 shows the performance comparison between the proposed algorithm and the raw and modified semi-supervised algorithms against the variation of the percentage of fingerprinting (i.e. calibration) load. The performance is also compared with the interpolation formulation considered in [8]. The crowd sourced information is set to 20% and localization requests are set to 7%. The comparison shows a much better performance for the the proposed algorithm at low percentage of fingerprints as depicted in Figure 3.9. However, the raw semi-supervised approach and interpolation formulation of [8] dominates at relatively higher percentage of fingerprinting data, which is expected. Nonetheless, this does not demerit the proposed unsupervised scheme with geometry perturbation because it is meant
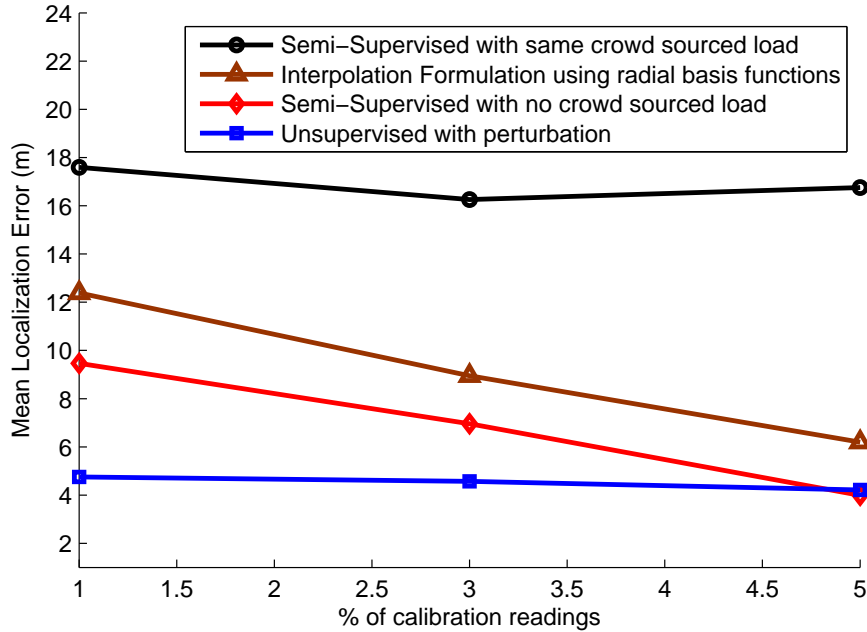
Figure 3.9: Mean localization error against the percentage of calibration readings to operate at the least level of fingerprinting load (less than 1 %), at which it significantly dominates by around 60 % improvement factor.

3.4.3 Variation of Crowd Sourced Information

Figure 3.10 shows the mean localization error plotted against the increasing percentage of crowd sourced readings for the proposed unsupervised scheme with geometry perturbation and the modified semi-supervised algorithm. The fingerprinted readings are less than 1% and the localization is done for 15 requests (7% of the total number of grid points). It can be observed that the error remains approximately stable for both algorithms as the percentage of crowd sourced information is increased. This is usually expected since increasing the unlabeled data in unsupervised learning do not usually improve the performance. This re-
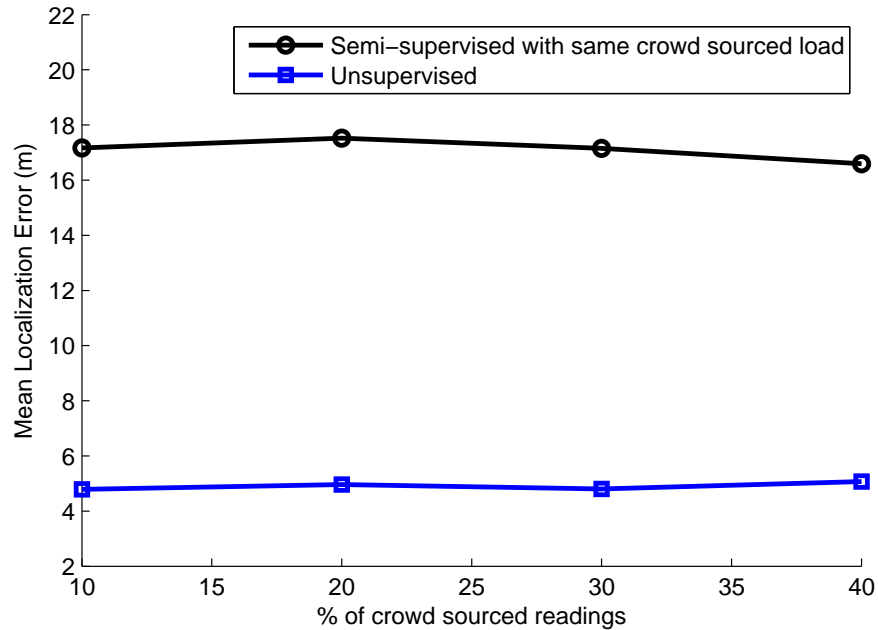
Figure 3.10: Comparison of unsupervised and semi-supervised algorithms with same crowd sourced information

sult is very important as it means that the proposed unsupervised algorithm does not need to wait for collecting a large number of crowd sourced readings before to perform localization. This allows the use of real-time crowd sourced readings (i.e. readings collected at the same time or very short time before the localization requests) for localization, which naturally adapts the accuracy of the algorithm to temporal variations of RSS readings.

3.4.4 Variation of Localization Requests

Figure 3.11 shows the mean localization error plotted against the increasing percentage of localization requests. The fingerprinting load is set to less than 1% and the crowd sourced information is set to 10%. An almost stable trend in the mean localization error can be observed. The same trend can also be observed

for the semi-supervised approaches. The result obtained from this figure is again very important as it shows that the proposed unsupervised algorithm does not need to collect a large number of requests to perform a better localization. It can rather perform one localization requests as good as many without affecting the performance.
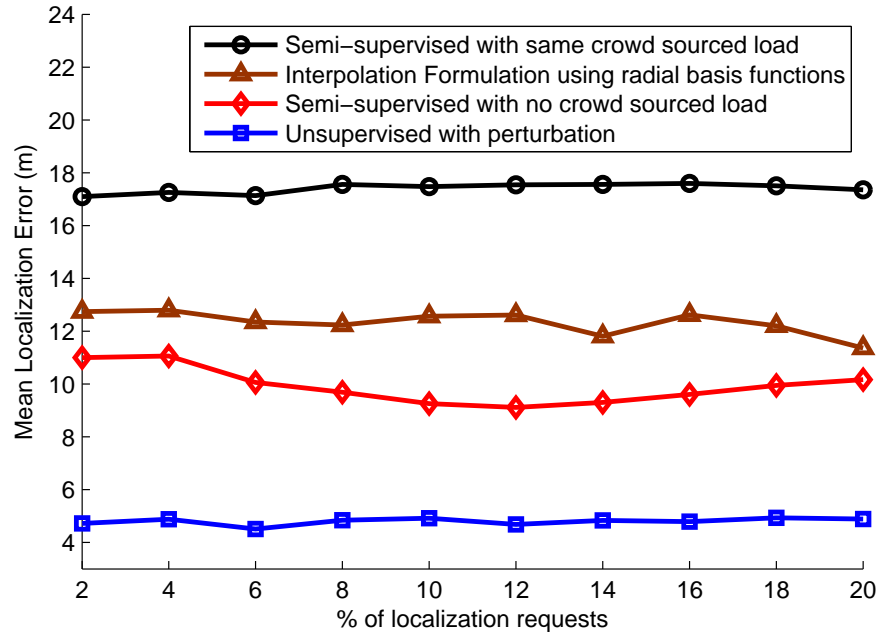
Figure 3.11: Mean localization error against the percentage of localization requests

3.5 Performance Improvement by Clustering

The testing results of previous section show that the performance achieved by using unsupervised technique with geometry perturbation is less than 5 m. The curves in Figure 3.9 show the performance in case of increasing calibration readings. If by somehow the indoor localization system needs to be operated at this range of calibration readings (which is probably less than the percentage used

in semi-supervised approaches to obtain this level of performance), this section describes the clustering approach considered to further improve the performance.

The data collected, as mentioned earlier, consists of RSS readings (calibration readings or fingerprints, crowd sourced readings and localization requests) and plan coordinates of the indoor area. The clustering of this data requires the selection of fingerprints at regular intervals throughout the indoor area. This is necessary to avoid the clustering errors (will be described shortly) to much extent. The clustering of data is based on the minimum Euclidean distance criterion as opposed to clustering by affinity propagation [29]. The clustering by affinity propagation used in [21, 23] considers the fingerprints at all the, N, grid points. So, in addition to the clustering, we know the corresponding coordinates also. The two main reasons why clustering by affinity propagation [29] is not used here are following.

1. The clustering is done independently in each of the readings data set $\mathcal{X}$ and coordinates data set $\mathcal{Z}$.

2. The clustered RSS readings (consist of crowd sourced readings and localization requests) do not have any pairwise correspondence with the coordinates.

In the light of above reasons, the clusters formed in the RSS readings domain may not overlap perfectly with the clusters in coordinates domain. The localization performance is little worse when the size of the cluster is small since it poses more chances of spillage of RSS reading outside the cluster. This effect and its solution is discussed in the upcoming subsection.

In this work, the clustering of only crowd sourced data and localization requests is done. The corresponding coordinates for these readings are unknown. The localization error together with the clustering error act as the main source in performance degradation. The idea of mismatch of the formed clusters from the source (readings) data set to the clusters from the destination (coordinates) data set is shown in Figure 3.12. It can be observed that some RSS readings associated
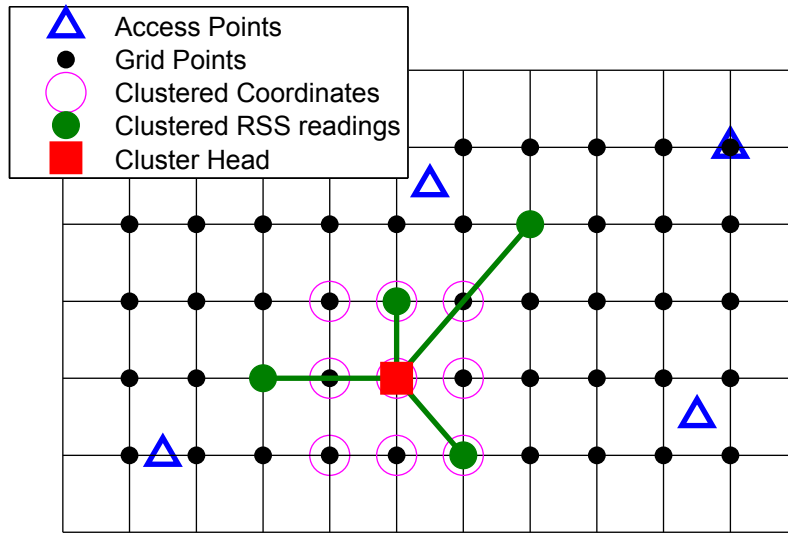
Figure 3.12: Pictorial demonstration of clustering error. The hollow circles represent the clustering of coordinates. The clustering of RSS readings is represented by filled circles

with the cluster may fall outside of it. However, the clustering here helps in a way that the localization region is constricted to much smaller area, which forces the location estimation to be done in this area. This strictly avoids false matches to other regions of the indoor area and the error incurred in this case is probably less.

Moving on with the clustering approach proposed here, the calibration readings set $\mathcal{C}$, given by (3.2), is restated as following along with the corresponding

coordinates:

$$\mathcal{C} = \left\{ \begin{bmatrix} c_1^{(1)} \\ c_2^{(1)} \\ \vdots \\ c_R^{(1)} \end{bmatrix}, \begin{bmatrix} c_1^{(2)} \\ c_2^{(2)} \\ \vdots \\ c_R^{(2)} \end{bmatrix}, \cdots, \begin{bmatrix} c_1^{(f)} \\ c_2^{(f)} \\ \vdots \\ c_R^{(f)} \end{bmatrix} \right\} \tag{3.31}$$

$$\mathcal{P}_{\mathcal{C}} = \left\{ \mathbf{p}_{c_1}, \mathbf{p}_{c_2}, \cdots, \mathbf{p}_{c_f} \right\} \tag{3.32}$$

For forming the clusters, the calibration readings in set $\mathcal{C}$ act as cluster heads. So the number of clusters is equal to the cardinality of set $\mathcal{C}$. Once the cluster heads are selected, the Euclidean distance of each of the crowd sourced readings is calculated from all of them. The crowd sourced reading with the minimum distance to the ith cluster head, $\mathbf{c}_i$, is associated with it. Let $\mathcal{O}_{\mathcal{H}_i}$ denotes the set containing the crowd sourced readings falling in the ith cluster. The association of the crowd sourced reading to the ith cluster $\mathcal{O}_{\mathcal{H}_i}$, is then defined as:

$$\mathcal{O}_{\mathcal{H}_i} = \left\{ \bigcup_{\mathbf{o}_j \in \mathcal{O}, k=i} \mathbf{o}_j \middle| \min_{\mathbf{c}_k \in \mathcal{C}} \|\mathbf{o}_j - \mathbf{c}_k\|_2 \right\} \tag{3.33}$$

The $\mathbf{o}_j$'s belonging to the ith cluster are thus accumulated in $\mathcal{O}_{\mathcal{H}_i}$. Let $\mathcal{L}_{\mathcal{H}_i}$ denotes the set containing localization requests, which fall in the ith cluster. The localization requests are clustered similarly by using:

$$\mathcal{L}_{\mathcal{H}_i} = \left\{ \bigcup_{\mathbf{l}_j \in \mathcal{O}, k=i} \mathbf{l}_j \middle| \min_{\mathbf{c}_k \in \mathcal{C}} \|\mathbf{l}_j - \mathbf{c}_k\|_2 \right\} \tag{3.34}$$

The clustering of plan coordinates is also based on the minimum Euclidean distance criterion. The coordinates present in set $\mathcal{P}_\mathcal{C}$ are cluster heads, whereas the remaining coordinates are clustered using:

$$\mathcal{P}_{\mathcal{H}_i} = \left\{ \bigcup_{\mathbf{z}_j \in \mathcal{Z}_r, k=i} \mathbf{z}_j \Big| \min_{\mathbf{p}_{c_k} \in \mathcal{P}_\mathcal{C}} \|\mathbf{z}_j - \mathbf{p}_{c_k}\|_2 \right\} \tag{3.35}$$

Figure 3.13 shows the clustering of plan coordinates. The number of clusters
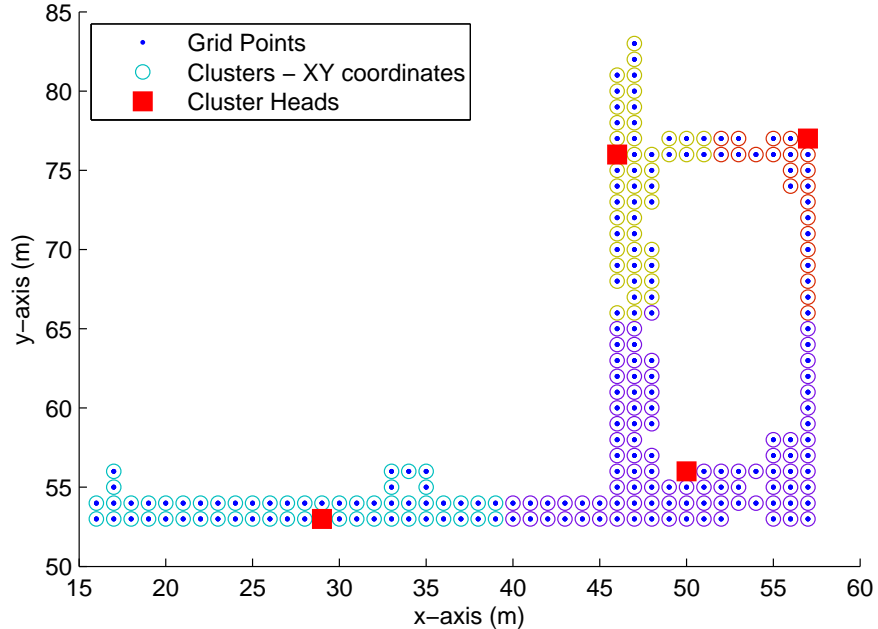
Figure 3.13: Clustering of the plan coordinates. The hollow circles represent the clustering of coordinates. The clusters are identified by separate colors. The number of clusters considered here are 4

shown here are 4, which correspond to 4 cluster heads. Figure 3.14 shows the clustering of plan coordinates together with RSS readings. These figures show the actual indoor plan considered for testing.

Once the clustering of coordinates and RSS readings is done independently,
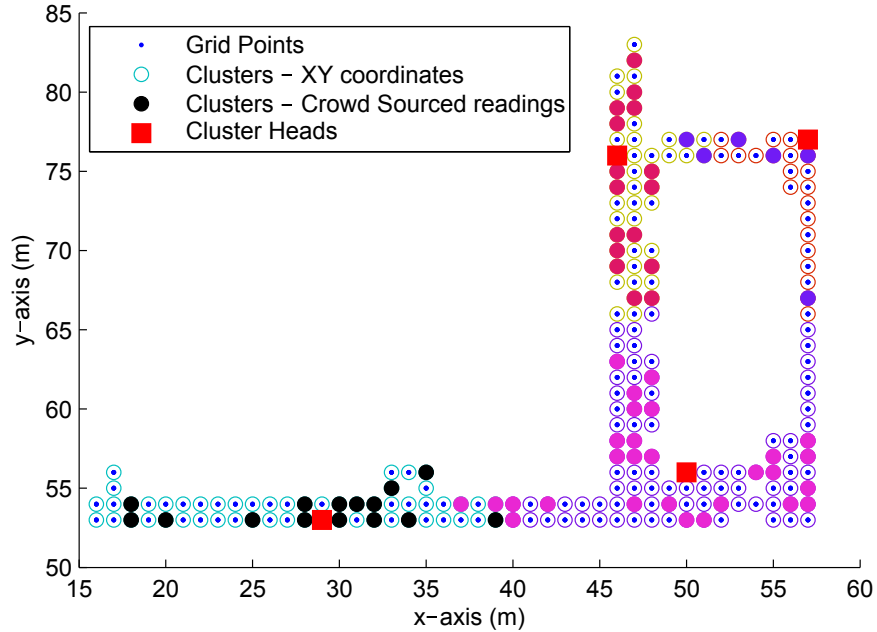
Figure 3.14: Clustering of the crowd sourced readings. The filled circles represent the clustered RSS readings. The hollow circles represent the clustered coordinates. The clusters are identified by separate colors. Localization requests are not shown here. However, these are also clustered in the same way i.e. associated with the minimum distance cluster head

the clusters corresponding to the localization requests are identified and the data sets are built up. Note that only the clusters containing localization requests are picked up. This has an added advantage that the algorithm does need to be run for the whole indoor area instead it finds the mappings in only small portion of the area. This reduces the running cost of the algorithm.

Consider user(s) in a region corresponding to the ith cluster. The ith cluster contains the crowd sourced readings identified by set $\mathcal{O}_{\mathcal{H}_i} \subseteq \mathcal{O}$, and localization requests by $\mathcal{L}_{\mathcal{H}_i} \subseteq \mathcal{L}$. The unsupervised manifold alignment algorithm with geometry perturbation described in 3.2 requires the source and destination data sets be built up according to Equations (3.7) and (3.8), respec-

tively. Based on the ith cluster containing localization request(s), the source data set becomes $\{\mathbf{c}_1, \cdots, \mathbf{c}_f, \mathcal{O}_{\mathcal{H}_i}, \mathcal{L}_{\mathcal{H}_i}\}$. Similarly, the destination data set becomes $\{\mathbf{p}_{c_1}, \cdots, \mathbf{p}_{c_f}, \mathcal{P}_{\mathcal{H}_i}\}$. These data sets are then passed to the indoor localization algorithm described in Section 3.3. The algorithm then provides position estimates of the user(s).

Figure 3.15 describes the comparison of mean localization error for clustering the available data as well as without clustering it. The curves shown in the figure are obtained by several runs of the algorithm. The calibration points considered were also varied during the testing. However, besides varying the calibration readings it was made sure that the selection of these points remain regular throughout the coordinate geometry.
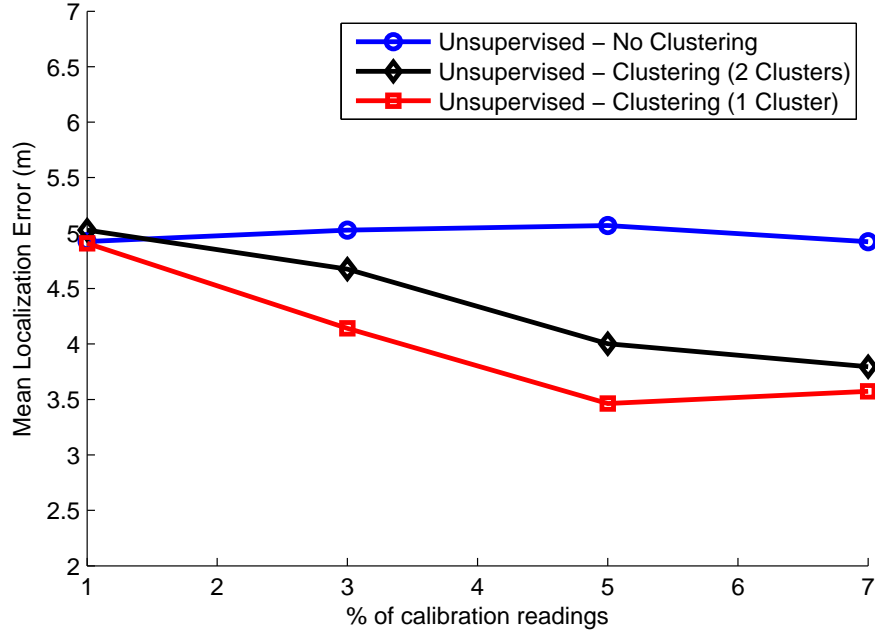
Figure 3.15: Comparison of clustering with non-clustering approach

One of the curves, indicated in the above Figure, is plotted by combining the crowd sourced readings and localization requests from two clusters. This results in increased localization error as compared to picking up only one cluster. This is due to the increased area as well as the clustering error resulting from picking up wrong cluster. Due to the well-defined geometry of coordinates, the clusters in the coordinates domain are also well-defined. However, for RSS readings this is not the case. The picking up of 2 minimum distance clusters for RSS reading (localization request) may not end up with 2 adjacent clusters in the spatial domain. The localization request thus remains outside of both of the picked up clusters if observed in the spatial domain. Thus the localization error is increased. Figure 3.16 shows the scenario of picking up 2 minimum distance clusters, where the localization request resides outside of these clusters.
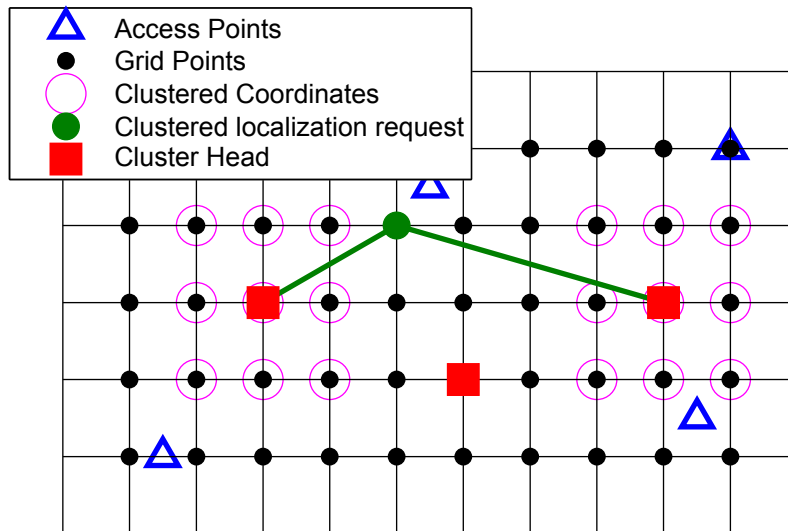
Figure 3.16: Pictorial view of localization request residing outside of the 2 minimum distance picked up clusters. The three cluster heads are shown here. Based on the minimum distance of the localization request with the cluster heads, the 2 picked up clusters in the spatial domain are shown. The destination data set built up here comprises of the coordinates from these clusters only

57

3.5.1 Clustering by Weighted Centroid Approach

According to the aforementioned details, the clusters formed by minimum Euclidean distance criterion helps to reduce the complexity of the algorithm while achieving good performance at some percentage of calibration readings (approx. 7%). From Figure 3.15 it can be observed when the number of clusters (or equivalently the calibration readings) are increased, the performance degrades (at 7% here). This is due to the clustering errors (Note: when we have more fingerprints, the size of cluster reduces). More of the RSS readings clustered fall outside the coordinates clustered underneath. As mentioned earlier, clustering in the coordinates domain is well defined, i.e the neighboring clusters have well defined boundaries, whereas this is not the case in RSS domain. The proposed method to reduce this error makes use of weighted centroid approach. In this approach, the best two or more clusters (based on the minimum Euclidean distance criterion) for the localization request are picked up and localization algorithm is run independently in the picked up clusters. This process is repeated for each localization request. Correspondingly, two or more estimated positions are obtained for each localization request. The centroid of these estimated positions is calculated to obtain the position estimate, $\hat{\mathbf{p}}_{l_i}$, for the localization request $\mathbf{l}_i$.

Figure 3.17 shows the trend in mean localization error as the calibration readings are increased. It can be observed that by increasing the number of calibration readings (corresponds to the number of clusters), the mean localization error is decreased. The highest weight is given to the first best matched cluster. The best

performance is achieved when size of the cluster reduces (at comparatively large
number of calibartion readings, i.e. 7 % readings in this case). So the clustering
with the weighted centroid approach outperforms the no clustering and regular
clustering cases.
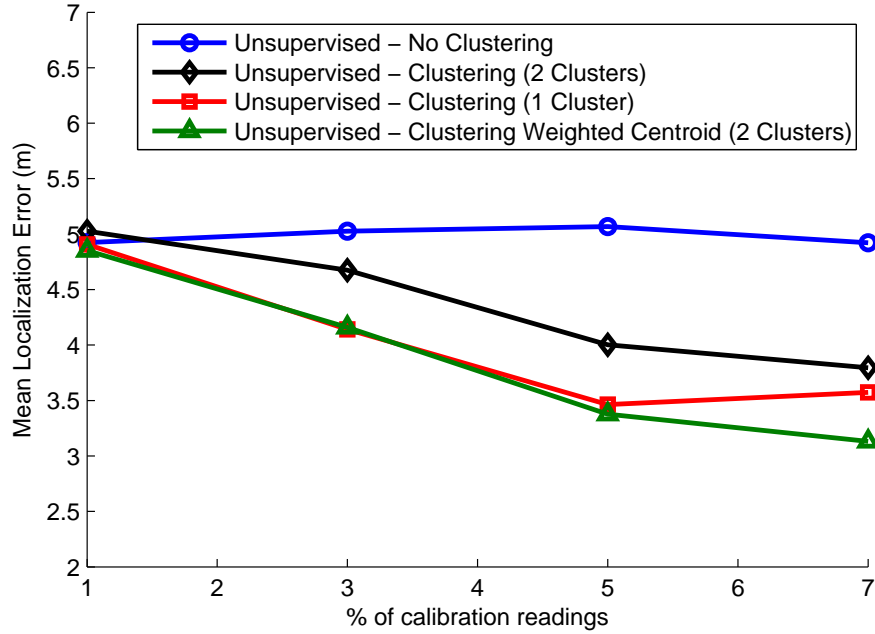
Figure 3.17: Comparison of the regular clustering with the weighted centroid
approach

Table 3.2 shows the numerical values of the mean localization error of the
curves plotted in Figure 3.17. Based on the numerical values, the percentage
improvement for clustering with weighted centroid approach (as compared to no
clustering case) in mean localization error is 17.3 % at just 3 % of the fingerprinting
load followed by 33.3 % at 5 % and 36.4 % at 7 % of the fingerprinting load.

Table 3.2: Comparison of clustering variants for proposed unsupervised technique considering calibration readings shown in Figure 3.17

Variant	1%	3%	5%	7%
	Mean Loc. Error (m)			
No clustering	4.92	5.03	5.07	4.92
Clustering (Combining 2 clusters)	5.03	4.68	4.00	3.80
Clustering (1 cluster)	4.91	4.14	3.46	3.57
Clustering with weighted centroid (2 clusters)	4.85	4.16	3.38	3.13

3.6   Chapter Summary

This chapter describes the indoor localization scheme that employs unsupervised manifold alignment using the environment's plan coordinates as destination data set. The proposed method employs some crowd sourced information and as low as 1% fingerprinting load (only 2 fingerprints in our case) that is only used to perturb the local geometries in the plan coordinates data set in order to make them unique. The proposed algorithm was shown to achieve less than 5 m mean localization error with as low as 1% fingerprinting load and limited crowd sourced information, when the semi-supervised localization approaches achieve around 10 m mean error and worse with the same level of available information. Moreover, testing of the algorithm using many random selections of localization requests and crowd sourced readings shows that the algorithm is robust to changes in such information and is thus scenario independent. The results also show that the proposed geometry perturbation introduced to provide uniqueness in the spatial domain is a corner stone in achieving this significant improvement compared to the conventional unsupervised manifold alignment scheme.

The additional methodology makes use of clustering to further improve the

performance if the system needs to be operated at some higher percentage of fingerprints (obviously this range is low than the one used in semi-supervised approaches for comparable performance). The clustering with weighted centroid approach shows better performance as compared to no clustering and regular clustering approaches.

CHAPTER 4

RADIO MAP ESTIMATION

Chapter 3 described the solution of indoor localization problem using unsupervised manifold alignment framework with geometry perturbation. The output of the algorithm provides position estimates for the localization requests. The localization requests (RSS values) along with the corresponding position estimates help to estimate the complete radio map of an indoor environment.

This chapter describes the construction of whole radio map from very limited amount of information, which includes only few fingerprints, few localization requests and plan coordinates of the indoor area. The estimation of radio map from above mentioned information can be regarded as the by-product of this system since it does not need any extra information. The following sections describe the problem setup and solution using linear estimation.

4.1 Estimation Problem Setup

This section describes the setting up of problem for radio map estimation. As mentioned earlier, for radio map estimation, the calibration readings (fingerprints), few localization requests and plan coordinates of the indoor environment are required. The fingerprints and plan coordinates are already available. When the system is deployed in the indoor environment, the localization requests are put up during normal operation of the system. The position estimates for these localization requests are obtained as described in Chapter 3. The following describes the problem setup for linear estimation.

The continuous running of the indoor localization algorithm provides the position estimates for the localization requests. After successive iterations of the algorithm, the RSS readings get accumulated at some positions. The accumulated RSS readings are averaged at those positions after fixed number of iterations. So, we have few positions with calibration readings (fingerprints) and few positions with averaged RSS readings. Note that the averaged RSS readings at corresponding positions may be different from the actual fingerprints at those positions. The remaining positions do not contain any RSS readings and thus the RSS values are estimated at those positions. Figure 4.1 represents the scenario of gathering RSS readings after fixed number of iterations of the indoor localization algorithm. The averaged RSS readings are appended to the calibration readings set $\mathcal{C}$. So, the calibration readings and averaged RSS readings with corresponding coordinates are treated as labeled data in the estimation problem. Let set $\mathbf{\Psi}$ represents this

Coordinates		I_1	I_2	I_3	$\cdots$	$\cdots$	I_{t-1}	I_t	RSS_{avg}
$x^{(1)}y^{(1)}$		X		X			X		a_1
$x^{(2)}y^{(2)}$	RSS		X					X	RSS
$x^{(3)}y^{(3)}$									
$\vdots$	RSS			X					RSS
$x^{(i)}y^{(i)}$		X		X			X		a_i
$x^{(j)}y^{(j)}$									
$x^{(k)}y^{(k)}$									
$\vdots$	RSS								RSS
$x^{(N-2)}y^{(N-2)}$			X						a_{N-2}
$x^{(N-1)}y^{(N-1)}$	RSS						X		RSS
$x^{(N)}y^{(N)}$		X		X				X	a_N

Figure 4.1: Data collection through continuous running of the indoor localization algorithm. The highlighted RSSs represent the fingerprints. The symbols 'X' represent the RSS readings (localization requests), which are put during successive iterations. These all are R dimensional vectors

labeled information. This is given as:

$$
\boldsymbol{\Psi} = \left\{ \begin{bmatrix} c_1^{(1)} \\ c_2^{(1)} \\ \vdots \\ c_R^{(1)} \end{bmatrix}, \cdots, \begin{bmatrix} c_1^{(f)} \\ c_2^{(f)} \\ \vdots \\ c_R^{(f)} \end{bmatrix}, \begin{bmatrix} a_1^{(1)} \\ a_2^{(1)} \\ \vdots \\ a_R^{(1)} \end{bmatrix}, \cdots, \begin{bmatrix} a_1^{(b)} \\ a_2^{(b)} \\ \vdots \\ a_R^{(b)} \end{bmatrix} \right\} \tag{4.1}
$$

The first f elements in set $\boldsymbol{\Psi}$ represent the fingerprints and next b elements represent the averaged RSS readings. The cardinality of this set is $(f + b)$, where $(f + b) \ll N$.

The coordinates corresponding to the RSS readings in set $\boldsymbol{\Psi}$ are given in set $\mathcal{P}_\Psi$:

$$
\mathcal{P}_\Psi = \{\mathbf{p}_{c_1}, \cdots, \mathbf{p}_{c_f}, \hat{\mathbf{p}}_{a_1}, \cdots, \hat{\mathbf{p}}_{a_b}\} \tag{4.2}
$$

The sequence of the elements in set $\mathcal{P}_\Psi$ is same as appearing in set $\boldsymbol{\Psi}$, that is, the first f elements are the corresponding coordinates of the calibration readings and next b elements are the positions where accumulated RSS readings are averaged.

From equations (4.1) and (4.2), this can be inferred that the RSS readings are known at the labeled $(f + b)$ positions. Now, we need to estimate the RSS values at remaining positions of the indoor environment. The estimation is done by considering RSS readings from one AP at a time. So, the total information from k^{th} AP can be divided into two column vectors, $\mathbf{v}_k$, the vector of unknown RSS values and $\mathbf{u}_k$, the vector of known RSS values. For k^{th} AP, the labeled RSS values, picked up from the set $\boldsymbol{\Psi}$, are given as:

$$\mathbf{u}_k = \left[\begin{array}{cccccc} c_k^{(1)} & \cdots & c_k^{(f)} & a_k^{(1)} & \cdots & a_k^{(b)} \end{array} \right]^T \tag{4.3}$$

The size of vector $\mathbf{u}_k$ is $(f + b) \times 1$. There are $(N - f - b)$ remaining positions where RSS values corresponding to the kth AP are to be determined. So, the size of vector $\mathbf{v}_k$ is $(N - f - b) \times 1$. The estimation problem is thus:

$$\hat{\mathbf{v}}_k = E[\mathbf{v}_k | \mathbf{u}_k] \tag{4.4}$$

The linear least-mean-squares estimator [34] is then used to solve the conditional expectation in (4.4). This is described in the following section.

4.2 Linear Estimation

The solution of conditional expectation given by Equation (4.4) is hard to get in closed form [34]. So the solution is obtained by using linear least-mean-squares estimator described as follows. Consider RSS values from k^{th} AP, the linear least-mean-squares estimator of $\mathbf{v}_k$ given $\mathbf{u}_k$ is given as:

$$\hat{\mathbf{v}}_k = \mathbf{R}_{v_k u_k} \mathbf{R}_{u_k}^{-1} \mathbf{u}_k \tag{4.5}$$

where, $\mathbf{R}_{v_k u_k}$ and $\mathbf{R}_{u_k}$ are the covariance matrices for the readings from k^{th} AP.

Once the matrices $\mathbf{R}_{v_k u_k}$ and $\mathbf{R}_{u_k}$ are known, the RSS values at the remaining positions can be determined. Now, the main task is to determine $\mathbf{R}_{v_k u_k}$ and $\mathbf{R}_{u_k}$. The information available to us is labeled data as in set $\mathbf{\Psi}$, their corresponding coordinates in set $\mathcal{P}_\Psi$ and remaining coordinates of the indoor area. As mentioned in Chapter 3, the readings and coordinates data sets used in unsupervised manifold alignment problem, have the same underlying correlation pattern. Note that the points closer to each other have stronger correlation as compared to distant points. Taking this fact into account, two approaches are considered to approximate $\mathbf{R}_{v_k u_k}$ and $\mathbf{R}_{u_k}$. The first approach does this approximation by heat kernel (HK) and the second approach by Locally Linear Embedding (LLE) [31]. $\mathbf{R}_{v_k u_k}$ represents the relationship between unknown values in vector $\mathbf{v}_k$ and known values in vector $\mathbf{u}_k$. To obtain this relationship, the coordinates of the indoor plan are partitioned into two sets i.e. one set contains the coordinates corresponding to the labeled data as

given by Equation (4.2) and the second set contains the coordinates, where RSS values are to be determined. The coordinates in the second set are, in fact, the remaining coordinates of the indoor plan and are accumulated in set $\mathcal{Q}$.

$$\mathcal{Q} = \{\mathbf{q}_1, \mathbf{q}_2, \cdots, \mathbf{q}_{N-f-b}\} \tag{4.6}$$

$\mathbf{R}_{u_k}$ represents the relationship between the knowns, that is, RSS values corresponding to the kth AP as indicated by the vector $\mathbf{u}_k$ in Equation (4.3). Following subsections describe the approaches to approximate the matrices $\mathbf{R}_{v_k u_k}$ and $\mathbf{R}_{u_k}$.

4.2.1   Approximation by Heat Kernel

The heat kernel calculates the weight between i^{th} and j^{th} elements by the following equation:

$$w_{ij} = e^{-\frac{d_{ij}^2}{\gamma}} \tag{4.7}$$

where, d_{ij} is the Euclidean distance between the ith and j^{th} elements. The elements belong to the same set when approximating $\mathbf{R}_{u_k}$ and to different sets in case of $\mathbf{R}_{v_k u_k}$. The value of γ chosen here is such that all the elements fall within 10 % of the maximum Euclidean distance computed above.

Approximation of $\mathbf{R}_{v_k u_k}$

The Euclidean distance, d_{ij}, is computed between the coordinates. The ith coordinate pair is taken from set $\mathcal{Q}$ while the jth coordinate pair is taken from set $\mathcal{P}_\Psi$. The heat kernel given by Equation (4.7) then computes the weight between the

unknown and known elements. The entry $w_{ij}^{v_k u_k}$ is the ij^{th} entry of the matrix $\mathbf{R}_{v_k u_k}$ i.e.

$$\mathbf{R}_{v_k u_k} = \begin{bmatrix} w_{11}^{v_k u_k} & w_{12}^{v_k u_k} & \cdots & w_{1(f+b)}^{v_k u_k} \\ w_{21}^{v_k u_k} & w_{22}^{v_k u_k} & \cdots & w_{2(f+b)}^{v_k u_k} \\ \vdots & \vdots & \ddots & \vdots \\ w_{(N-f-b)1}^{v_k u_k} & w_{(N-f-b)2}^{v_k u_k} & \cdots & w_{(N-f-b)(f+b)}^{v_k u_k} \end{bmatrix} \qquad (4.8)$$

The size of this matrix is $(N - f - b) \times (f + b)$, which corresponds to the number of elements in $\mathbf{v}_k$ and $\mathbf{u}_k$.

Approximation of $\mathbf{R}_{u_k}$

The Euclidean distance of each element in vector $\mathbf{u}_k$ is computed with all the elements in $\mathbf{u}_k$. The individual entries of $\mathbf{R}_{u_k}$ are then computed from the heat kernel given by Equation (4.7). The size of the matrix $\mathbf{R}_{u_k}$ is $(f + b) \times (f + b)$ and it is given as:

$$\mathbf{R}_{u_k} = \begin{bmatrix} w_{11}^{u_k} & w_{12}^{u_k} & \cdots & w_{1(f+b)}^{u_k} \\ w_{21}^{u_k} & w_{22}^{u_k} & \cdots & w_{2(f+b)}^{u_k} \\ \vdots & \vdots & \ddots & \vdots \\ w_{(f+b)1}^{u_k} & w_{(f+b)2}^{u_k} & \cdots & w_{(f+b)(f+b)}^{u_k} \end{bmatrix} \qquad (4.9)$$

The localization requests from users are obtained randomly in the indoor area, so the matrix $\mathbf{R}_{u_k}$ formed in Equation (4.9) from the labeled elements becomes

68

singular sometimes. The regularization term is added to $\mathbf{R}_{u_k}$ to account for the singularity, that is:

$$\mathbf{R}_{u_k} = \mathbf{R}_{u_k} + \epsilon \mathbf{I}_{(f+b)} \tag{4.10}$$

where, ϵ is a regularization factor and $\mathbf{I}_{(f+b)}$ is an $(f+b) \times (f+b)$ identity matrix.

This gives us approximations of the covariance matrices for the kth AP. After approximating $\mathbf{R}_{v_k u_k}$ and $\mathbf{R}_{u_k}$, the linear least-mean-squares estimator given by Equation (4.5) is used to estimate RSS values at all the positions other than the labeled positions.

The process is repeated to get these approximations for all the R APs present in the indoor environment. The RSS readings estimated at a position (grid point) from all the APs are then stacked as a vector to represent the estimated fingerprint at that position. So the estimated RSS values (estimated fingerprints) for all the $(N - f - b)$ positions (grid points) can be represented by the set $\boldsymbol{\Theta}$:

$$\boldsymbol{\Theta} = \left\{ \begin{bmatrix} \hat{v}_1^{(1)} \\ \hat{v}_2^{(1)} \\ \vdots \\ \hat{v}_R^{(1)} \end{bmatrix}, \begin{bmatrix} \hat{v}_1^{(2)} \\ \hat{v}_2^{(2)} \\ \vdots \\ \hat{v}_R^{(2)} \end{bmatrix}, \cdots, \begin{bmatrix} \hat{v}_1^{(N-f-b)} \\ \hat{v}_2^{(N-f-b)} \\ \vdots \\ \hat{v}_R^{(N-f-b)} \end{bmatrix} \right\} \tag{4.11}$$

or, in compact form as:

$$\boldsymbol{\Theta} = \{\boldsymbol{\theta}_1, \boldsymbol{\theta}_2, \cdots, \boldsymbol{\theta}_{N-f-b}\} \tag{4.12}$$

69

where, $\boldsymbol{\theta}_i$ represents the estimated fingerprint at the ith position or grid point.

4.2.2 Approximation by Locally Linear Embedding

The second approach considered for estimating the covariance matrices makes use of weight computation by Locally Linear Embedding (LLE) [31]. Out of several dimensionality reduction techniques, the LLE is used here since it strongly preserves the correlation between element and its neighbors. This is consistent with our data sets since they have the same underlying correlation pattern. Instead of using the nearest neighbors, the labeled data indicated by Equations (4.2) and (4.3) are used as neighbors for all the elements while approximating the covariance matrices. These elements include RSS values in set $\boldsymbol{\Psi}$ and corresponding coordinates in set $\mathcal{P}_{\boldsymbol{\Psi}}$. These act as neighbors while computing $\mathbf{R}_{v_k u_k}$ and $\mathbf{R}_{u_k}$. The procedure of obtaining the approximation of these matrices is described in the following.

Approximation of $\mathbf{R}_{v_k u_k}$

For $\mathbf{R}_{v_k u_k}$, all the elements in set $\mathcal{P}_{\boldsymbol{\Psi}}$ are used as neighbors for each element present in set $\mathcal{Q}$. The LLE then computes weight of the element $\mathbf{q}_i$ in set $\mathcal{Q}$ with all its neighbors in set $\mathcal{P}_{\boldsymbol{\Psi}}$ by the following relation:

$$\min_{w_{ij}^{v_k u_k} \forall \mathbf{p}_j \in \mathcal{P}_{\boldsymbol{\Psi}}} \left| \mathbf{q}_i - \sum_{\mathbf{p}_j \in \mathcal{P}_{\boldsymbol{\Psi}}} w_{ij}^{v_k u_k} \mathbf{p}_j \right|^2 \tag{4.13}$$

$$s.t. \sum_{\mathbf{p}_j \in \mathcal{P}_{\boldsymbol{\Psi}}} w_{ij}^{v_k u_k} = 1$$

where, $w_{ij}^{v_k u_k}$ is the weight computed by LLE between the ith and j^{th} elements in sets $\mathcal{P}_\Psi$ and $\mathcal{Q}$, respectively. This, in fact, is the ij^{th} entry of the matrix $\mathbf{R}_{v_k u_k}$. As mentioned in the previous subsection, the size of this matrix is $(N - f - b) \times (f + b)$. The structure of this matrix is same as shown by Equation (4.8) except for the fact that weights here are computed by LLE instead of heat kernels.

Approximation of $\mathbf{R}_{u_k}$

For approximating $\mathbf{R}_{u_k}$, each element in vector $\mathbf{u}_k$ uses all other elements in the same vector for computing weights by LLE, that is, for the ith element in vector $\mathbf{u}_k$, the remaining $(f + b) - 1$ elements act as its neighbors. The weights $w_{ij}^{u_k}$'s are given by the following relation:

$$
\min_{w_{ij}^{u_k} \forall u_k(j) \in \mathbf{u}_k \wedge (j \neq i)} \left| u_k(i) - \sum_{u_k(j) \in \mathbf{u}_k \wedge (j \neq i)} w_{ij}^{u_k} u_k(j) \right|^2
$$
$$
s.t. \sum_{u_k(j) \in \mathbf{u}_k \wedge (j \neq i)} w_{ij}^{u_k} = 1
$$

(4.14)

The weight $w_{ij}^{u_k}$ is the ij^{th} entry of the matrix $\mathbf{R}_{u_k}$. As mentioned earlier, the size of this matrix is $(f + b) \times (f + b)$. The structure of this matrix is same as shown by Equation (4.9) with the only difference that here the weights are computed by LLE.

As mentioned in the previous subsection, due to the random selection of localization requests, the matrix $\mathbf{R}_{u_k}$ becomes singular most of the times. So, the regularization term is added here also, as indicated by Equation (4.10), to account for the singularity in matrix $\mathbf{R}_{u_k}$. The RSS estimates for all the positions indi-

cated in set $\mathcal{Q}$ are obtained by using linear least-mean-squares estimator given by Equation (4.5).

The approximations for the matrices obtained above are used for estimating RSS readings corresponding to the kth AP. This process is repeated for all the APs present in the indoor environment. So, the estimated RSS values from all the APs at a grid point represent the estimated fingerprint at that point. The estimated fingerprints are represented in the same fashion as shown in Equations (4.11) and (4.12).

4.3   Testing Results

This section describes the performance testing of the proposed solution for radio map estimation. As mentioned earlier, the radio map construction relies on the data obtained from the indoor localization framework proposed in Chapter 3. This data includes few calibration readings, few localization requests with corresponding position estimates and plan coordinates of the indoor area.

The indoor floor plan considered is same as shown in Figure 3.7. The initial running of the indoor localization algorithm, described in Chapter 3, provides estimated positions for few localization requests, which help in estimating the radio map later. For performance evaluation, the root mean square (rms) error is plotted by comparing the actual fingerprints with the estimated one. The rms error calculation does not include the calibration readings (fingerprints) and is

given as:

$$err_{rms} = \sqrt{\frac{\sum_{i=1}^{b} \left(\mathbf{a}_i - \mathbf{c}_{\hat{p}_{a_i}}\right)^2 + \sum_{i=1}^{N-f-b} \left(\boldsymbol{\theta}_i - \mathbf{c}_i\right)^2}{R \times (N - f)}} \qquad (4.15)$$

The b elements in first summation represent the few localization requests gathered during initial running of the algorithm. $\mathbf{a}_i$ represents the averaged RSS readings at the ith grid point and $\mathbf{c}_{\hat{p}_{a_i}}$ represents the actual fingerprint at the same grid point. Similarly, for the second summation in Equation (4.15), $\boldsymbol{\theta}_i$ represents the estimated fingerprint at the ith grid point and $\mathbf{c}_i$ the actual fingerprint at the same point. In the testing, comparison between semi-supervised and unsupervised algorithms is considered along with different variations. The performance of the proposed solution is also checked by varying different parameters. The calibration readings and localization requests are randomly selected throughout the indoor area. The curves shown in the following are obtained by averaging over several runs of the algorithm.

4.3.1 Effect of varying Calibration Readings

Figure 4.2 shows the rms error plotted against the increasing percentage of calibration readings (fingerprints). The localization requests considered here are 1 %. The proposed indoor localization algorithm is run for fixed number of iterations (1 and 10 iterations shown here). The proposed radio map estimation is done for both the semi-supervised algorithm in [5] and proposed unsupervised indoor localization framework in Chapter 3. Figure 4.3 shows the similar curves but for approximation of the covariance matrices using LLE.
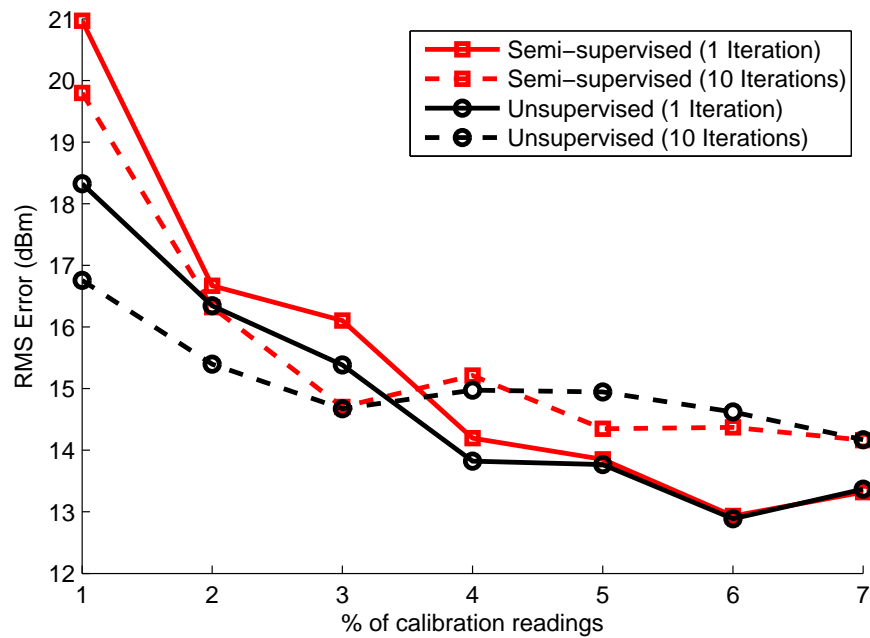
Figure 4.2: RMS error plotted against the increasing percentage of calibration readings using heat kernel approximation for covariance matrices
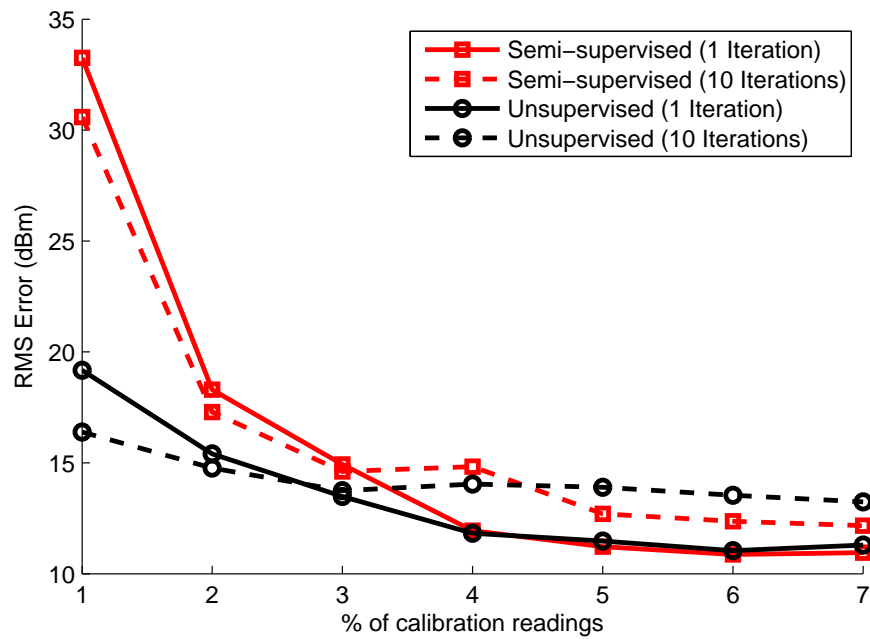

Figure 4.3: RMS error plotted against the increasing percentage of calibration readings using LLE approximation for covariance matrices

From Figures 4.2 and 4.3, this can be observed that the proposed unsupervised algorithm shows huge improvement in performance as compared to the semi-supervised approach at only 1% of fingerprinting load, 1% of localization requests and 1 iteration of the algorithms (1% in our case are only 2 points). Further improvement is observed after 10 iterations of the algorithm. However, for 10 iterations of the algorithm the performance starts to deteriorate after 3% of the calibration readings. This corresponds to the total labeled data of 13%, that is, almost 28 points out of total 219 points in the indoor environment considered here. This is consistent with the results and proves the fact that the proposed unsupervised algorithm is meant to operate at very low level of fingerprinting load. The same effect can also be observed by varying the localization requests while fixing the number of iterations to 1. The 10% localization requests with 1 iteration is almost equivalent to 1% localization requests with 10 iterations since both of them will provide almost the same number of position estimates. The comparison of these figures also show the better performance of using LLE approximations rather than heat kernel at low percentage of fingerprinting load.

4.3.2 Effect of including Localization Requests

Figure 4.4 shows the effect of including localization requests on rms error. The curves plotted here are again averaged over several runs of the algorithm. The proposed unsupervised framework for indoor localization is considered here for radio map estimation. The curves shown here are using LLE approximations of the
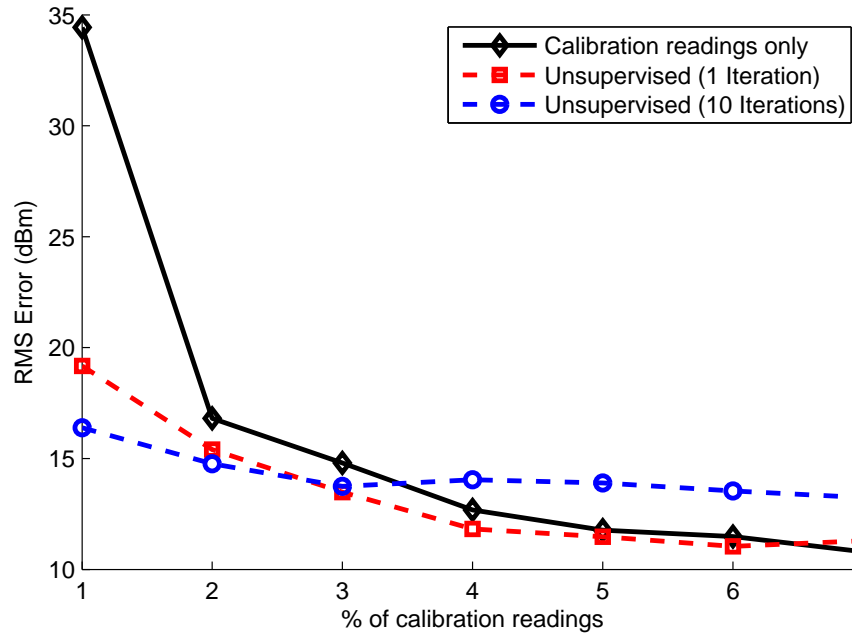
75

Figure 4.4: Effect of including localization requests in radio map estimation

covariance matrices. The localization requests considered are 1%. The algorithm

is run for 1 and 10 iterations. Another curve is plotted, which does not take into

account the localization requests and use only calibration readings to estimate

the radio map. The comparison of the curves show considerable improvement

in performance when localization requests are included as the labeled data for

radio map estimation. The performance improvement is really high at 1% of the

fingerprinting load. The percentage improvement in performance for 1 iteration

and 10 iterations of the algorithm is 44% and 52%, respectively, at 1% of the

fingerprinting load.

4.3.3 Effect of using Actual Fingerprints for Labeled Data at Estimated Positions

The indoor localization algorithm outputs position estimates for the localization requests, which are already in some error. This leaves us with the question, how far we are in estimating the radio map if we are not using actual fingerprints at the concerned positions or grid points? Figures 4.5 and 4.6 (using heat kernel and LLE approximations for covariance matrices respectively) show the comparison of including localization requests and corresponding position estimates with that of actual fingerprints at those estimated positions. The localization requests considered here again are 1% and the indoor localization algorithm is run for 1 iteration. The comparison of the curves show that we are not far away in rms error. The rms error, by not using actual fingerprints at concerned grid points, falls in between 1$\sim$2 dBm.
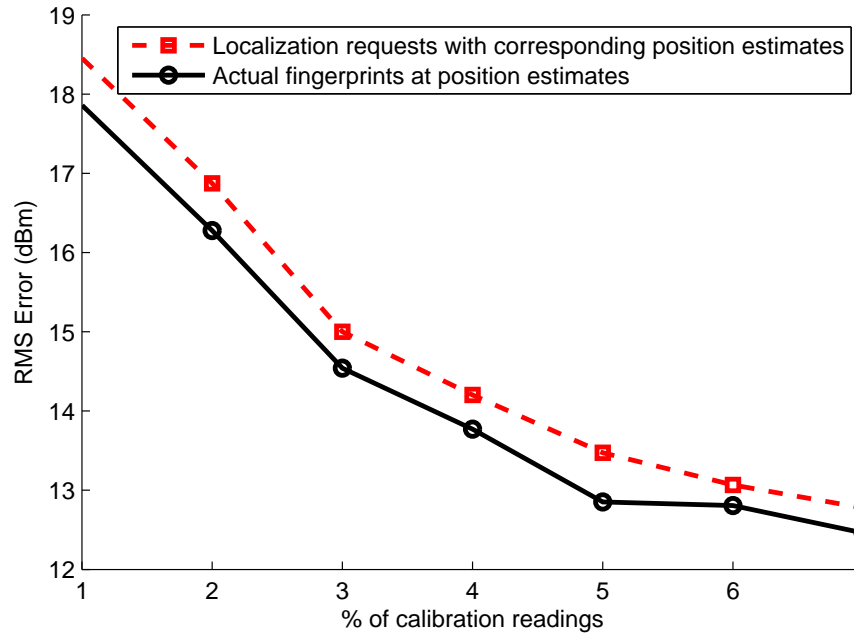
Figure 4.5: Effect of using actual fingerprints for labeled data at estimated positions using heat kernel approximation for covariance matrices
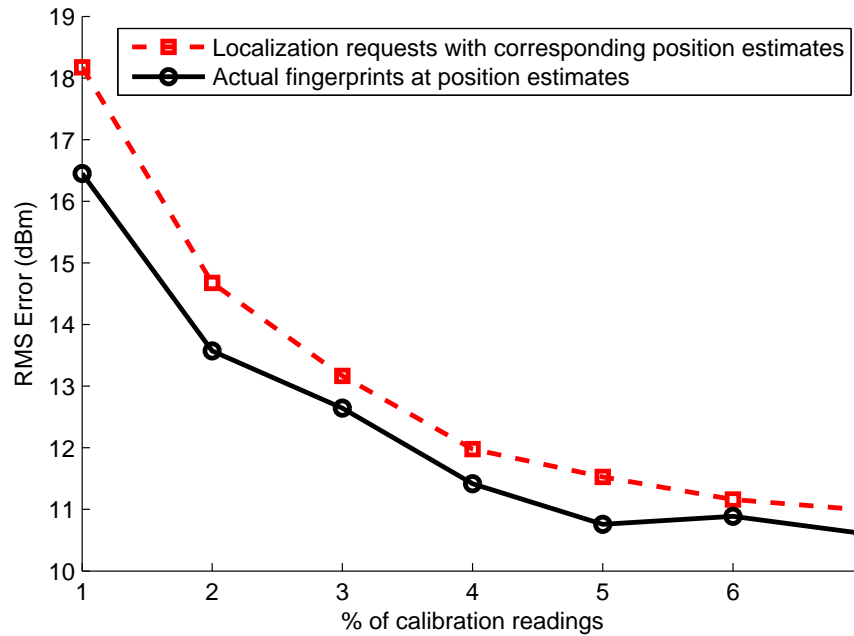

Figure 4.6: Effect of using actual fingerprints for labeled data at estimated positions using LLE approximation for covariance matrices

4.3.4   Pictorial view of Estimated RSS Readings

Figure 4.7 shows the actual RSS signal strengths measured from the first AP. The bright colors in larger filled circles show stronger signal strengths. The color and size of the circle also change with decreasing signal strength. The minute dots around top right corner of the figure shows no coverage by AP 1. The
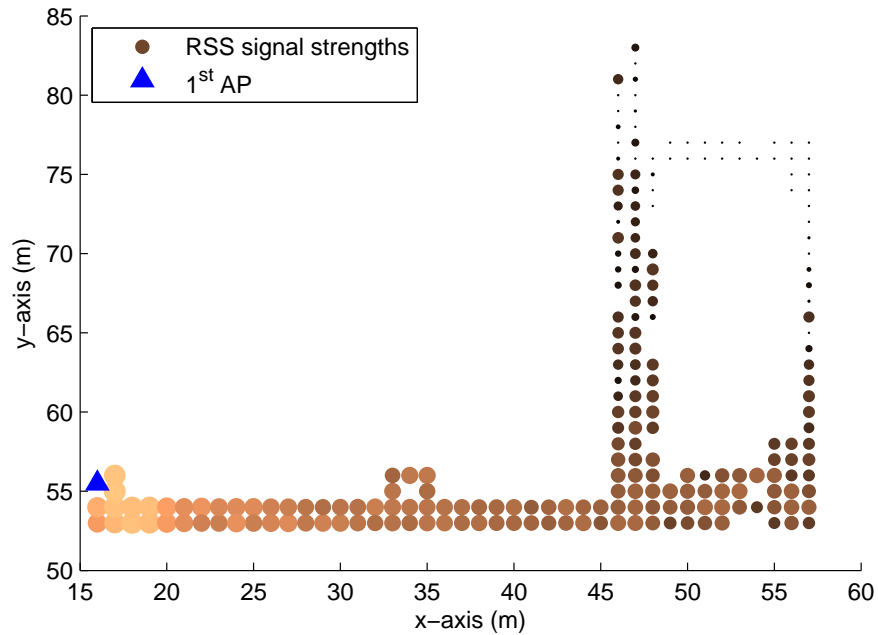
Figure 4.7: Radio Map showing actual RSS signal strengths measured from AP 1

localization requests considered are 1% and calibration readings (fingerprints) are also 1%. The estimated RSS signal strengths shown here consider approximation of covariance matrices by using LLE. The signal strength map obtained by 1 iteration of the indoor localization algorithm is shown in Figure 4.8. Figure 4.9 shows the similar map but with 10 iterations of the indoor localization algorithm.

Figure 4.8: Radio Map showing estimated RSS signal strengths for AP 1 (1 iteration)
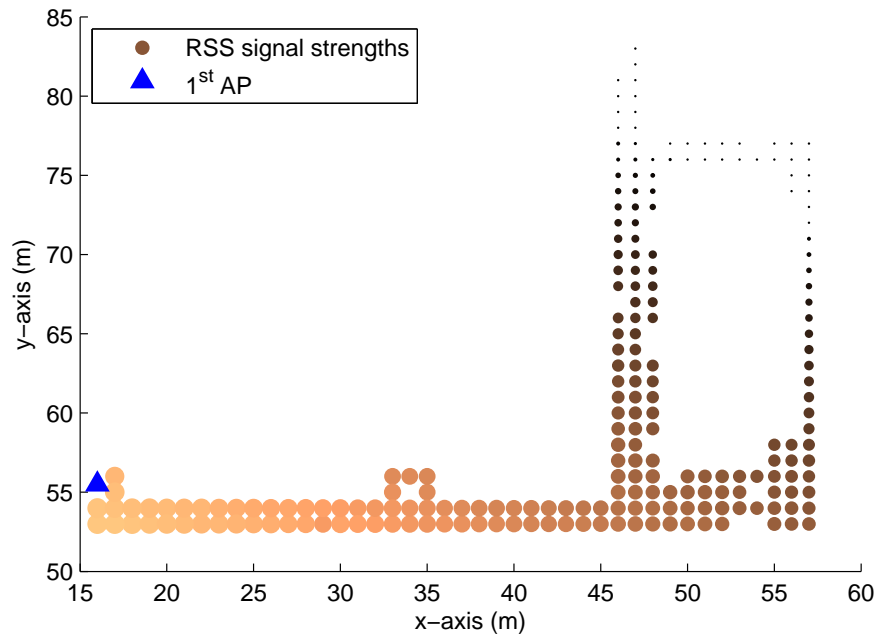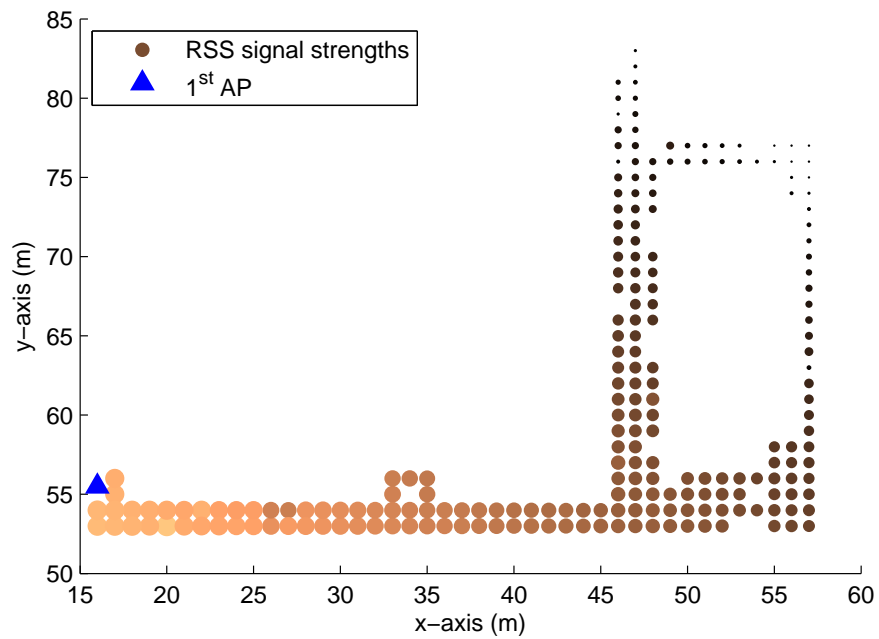

Figure 4.9: Radio Map showing estimated RSS signal strengths for AP 1 (10 iterations)

4.4   Chapter Summary

This chapter describes the proposed methodology for radio map estimation in the indoor environment. The calibration readings with few localization requests help in estimating the complete radio map of the indoor environment. This results in much better accuracy. The proposed unsupervised indoor localization framework shows better performance while doing radio map estimation as compared to the semi-supervised approach. Moreover, the performance greatly improves by increasing the iterations to 10. The percentage improvement is around 50% in this case at only 1% of the fingerprinting load. The comparison of using actual fingerprints at the estimated positions is also made with the averaged RSS readings at those positions. The difference of rms error around 1~2 dBm shows that we are not doing worse by including accumulated localization requests as labeled data.

CHAPTER 5

CONCLUSION AND FUTURE

WORK

5.1 Conclusion

The thesis described the important problem of indoor localization using RSS fingerprints from WLAN Access Points. The proposed solution using unsupervised manifold alignment framework with geometry perturbation almost eliminated the workload required for practical deployment of such systems. The overall contributions from this work can be summarized in the following points.

1. **Proposed indoor localization framework**

   The collection of very small number of fingerprints together with some crowd sourced readings, localization requests and plan coordinates of the indoor environment help in location sensing. The proposed solution shows remarkable performance at very small number of calibration load (approximately 1%).

The comparison with other semi-supervised techniques also shows good performance. The practical deployment of proposed indoor localization system in a new indoor environment does not require any initial setup time.

2. **Performance improvement by clustering**

The testing results show collection of fingerprints to a smaller number (greater than 1% but still less than the semi-supervised schemes for same level of performance). Further enhancement is done by using clustering approach. The clustering of data helps in performance improvement as well as it reduces complexity of the proposed technique. The proposed clustering solution does not need to consider the complete floor plan instead the clusters containing localization requests are picked up and location estimates are obtained.

3. **Radio map estimation**

The importance of radio coverage of an indoor environment motivated us to estimate the complete radio map of the indoor environment. The proposed solution does not need any extra information other than that of the already available few fingerprints and few localization requests. The inclusion of localization requests as labeled data greatly improves the performance. The comparison of using actual fingerprints at all the labeled positions is also made, which shows that we are doing little worse by using associated RSSs at obtained position estimates.

5.2 Future Work

The proposed indoor localization framework provides a way to eliminate the workload required to build fingerprinted databases. The practical implementation of the algorithm is quite simple in the real environment. This is obviously at the expense of increased localization error. This level of accuracy is specific to certain applications like path finding to certain spot, navigation in hospitals, airports, shopping malls. For assisting visually impaired people in the indoor area, more accuracy is required. Following points can be considered in future work to obtain high accuracy.

1. **Inclusion of TDoA**

   The RSS fingerprints are unique in the Wi-Fi space. The appending of TDoA fingerprints can make them more unique. The hybrid fingerprints can thus be used to estimate positions at the expense of increased workload and increased hardware requirements.

2. **Inclusion of sensory measurements**

   The readings from inertial sensors present in smart phones can be used in conjunction with RSS values measured by WNIC. The localization error can be decreased but at the expense of increased complexity and initial adaptation time required for deploying the indoor localization system in the real environment.

REFERENCES

[1] A. Kushki, K. N. Plataniotis, and A. N. Venetsanopoulos, "Kernel-based positioning in wireless local area networks," *IEEE Transactions on Mobile Computing*, vol. 6, no. 6, pp. 689–705, Jun. 2007.

[2] G. Sun, J. Chen, W. Guo, and K. R. Liu, "Signal processing techniques in network-aided positioning: A survey of state-of-the-art positioning designs," *Signal Processing Magazine, IEEE*, vol. 22, no. 4, pp. 12–23, 2005.

[3] H. Liu, H. Darabi, P. Banerjee, and J. Liu, "Survey of wireless indoor positioning techniques and systems," *IEEE Transactions on Systems, Man and Cybernetics, Part C (Applications and Reviews)*, vol. 37, no. 6, pp. 1067–1080, Nov. 2007.

[4] C. Drane, M. Macnaughtan, and C. Scott, "Positioning GSM telephones," *Communications Magazine, IEEE*, vol. 36, no. 4, pp. 46–54, 1998.

[5] Y. L. S. Sorour and S. Valaee, "Joint indoor localization and radio map construction with limited deployment effort," *submitted to IEEE Transactions on Mobile Computing*.

[6] C. Rizos, A. G. Dempster, B. Li, and J. Salter, "Indoor positioning techniques based on wireless LAN," 2007.

[7] S. Sorour, Y. Lostanlen, and S. Valaee, "RSS based indoor localization with limited deployment load," in *GLOBECOM*, 2012, pp. 303–308.

[8] J. Krumm and J. Platt, "Minimizing calibration efforts for an indoor 802.11 device location measurement system," 2003.

[9] J. Ham, D. Lee, and L. Saul, "Semisupervised alignment of manifolds," in *Proceedings of the Annual Conference on Uncertainty in Artificial Intelligence, Z. Ghahramani and R. Cowell, Eds*, vol. 10, 2005, pp. 120–127.

[10] Y. Pei, F. Huang, F. Shi, and H. Zha, "Unsupervised image matching based on manifold alignment," *IEEE Transactions on Pattern Analysis and Machine Intelligence*, vol. 34, no. 8, pp. 1658–1664, Aug. 2012.

[11] C. Wang and S. Mahadevan, "Manifold alignment without correspondence," in *IJCAI*, vol. 2, 2009, p. 3.

[12] International Organization for Standardization, International Electrotechnical Commission, and Institute of Electrical and Electronics Engineers, *Information technology telecommunications and information exchange between systems– local and metropolitan area networks– specific requirements. Part 11, Part 11,*. Geneva; New York: ISO : IEC ; Institute of Electrical and Electronics Engineers, 2012.

[13] H. Wang, S. Sen, A. Elgohary, M. Farid, M. Youssef, and R. R. Choudhury, "No need to war-drive: unsupervised indoor localization," in *Proceedings of the 10th international conference on Mobile systems, applications, and services.* ACM, 2012, pp. 197–210.

[14] A. Rai, K. K. Chintalapudi, V. N. Padmanabhan, and R. Sen, "Zee: zero-effort crowdsourcing for indoor localization," in *Proceedings of the 18th annual international conference on Mobile computing and networking.* ACM, 2012, pp. 293–304.

[15] Z. Yang, C. Wu, and Y. Liu, "Locating in fingerprint space: wireless indoor localization with little human intervention," in *Proceedings of the 18th annual international conference on Mobile computing and networking.* ACM, 2012, pp. 269–280.

[16] G. Shen, Z. Chen, P. Zhang, T. Moscibroda, and Y. Zhang, "Walkie-markie: indoor pathway mapping made easy," in *Proc. of USENIX NSDI*, 2013.

[17] R. Singh, L. Macchi, C. S. Regazzoni, and K. N. Plataniotis, "A statistical modelling based location determination method using fusion technique in WLAN," *Proc. IEEE IWWAN*, 2005.

[18] P. Bahl and V. N. Padmanabhan, "RADAR: an in-building RF-based user location and tracking system," in *INFOCOM 2000. Nineteenth Annual Joint Conference of the IEEE Computer and Communications Societies. Proceedings. IEEE*, vol. 2, 2000, pp. 775–784.

[19] N. K. Sharma, "A weighted center of mass based trilateration approach for locating wireless devices in indoor environment," in *MOBIWAC: Proceedings of the 4 th ACM international workshop on Mobility management and wireless access*, vol. 2, 2006, pp. 112–115.

[20] K. Kaemarungsi and P. Krishnamurthy, "Modeling of indoor positioning systems based on location fingerprinting," in *INFOCOM 2004. Twenty-third AnnualJoint Conference of the IEEE Computer and Communications Societies*, vol. 2, 2004, pp. 1012–1022.

[21] C. Feng, W. S. A. Au, S. Valaee, and Z. Tan, "Compressive sensing based positioning using RSS of WLAN access points," in *INFOCOM, 2010 Proceedings IEEE*, 2010, pp. 1–9.

[22] C. Feng, W. Au, S. Valaee, and Z. Tan, "Orientation-aware indoor localization using affinity propagation and compressive sensing," in *Computational Advances in Multi-Sensor Adaptive Processing (CAMSAP), 2009 3rd IEEE International Workshop on*, 2009, pp. 261–264.

[23] C. Feng, W. S. A. Au, S. Valaee, and Z. Tan, "Received-signal-strength-based indoor positioning using compressive sensing," *IEEE Transactions on Mobile Computing*, vol. 11, no. 12, pp. 1983–1993, Dec. 2012.

[24] H. Jamali-Rad, H. Ramezani, and G. Leus, "Sparse multi-target localization using cooperative access points," in *Sensor Array and Multichannel Signal Processing Workshop (SAM), 2012 IEEE 7th*, 2012, pp. 353–356.

[25] A. Kushki, P. K. N., and V. A. N., *WLAN Positioning Systems: Principles and Applications in Location-Based Services.* Cambridge University Press, 2012.

[26] E. Candes and M. Wakin, "An introduction to compressive sampling," *IEEE Signal Processing Magazine*, vol. 25, pp. 21–30, Mar. 2008.

[27] R. G. Baraniuk, "Compressive sensing [lecture notes]," *Signal Processing Magazine, IEEE*, vol. 24, no. 4, pp. 118–121, 2007.

[28] G. Kutyniok, "Compressed sensing: Theory and applications," *CoRR, vol. abs/1203.3815*, 2012.

[29] B. J. Frey and D. Dueck, "Clustering by passing messages between data points," *science*, vol. 315, no. 5814, pp. 972–976, 2007.

[30] H. Jamali-Rad and G. Leus, "Sparsity-aware multi-source TDOA localization," *IEEE Transactions on Signal Processing*, vol. 61, no. 19, pp. 4874–4887, Oct. 2013.

[31] S. T. Roweis, "Nonlinear dimensionality reduction by locally linear embedding," *Science*, vol. 290, no. 5500, pp. 2323–2326, Dec. 2000.

[32] R. Burden and J. Faires, *Numerical Analysis*, ser. Mathematics Series. Brooks/Cole, 2001.

[33] J. Nocedal and S. Wright, *Numerical Optimization*, ser. Springer series in operations research and financial engineering. Springer, 1999.

[34] A. Sayed, *Adaptive Filters.* Wiley, 2008.

Vitae

- Name: Khaqan Majeed

- Nationality: Pakistani

- Date of Birth: Aug 18, 1986

- Email: *khaqanmajeed@hotmail.com*

- Permenant Address: House#5, Street#4, Eden Palace Villas, Raiwind Road, Lahore, Pakistan

- Received Bachelor of Science (B.Sc.) degree in Electrical Engineering (with emphasis on Electronics and Communication) from University of Engineering and Technology (UET) Lahore, Pakistan in Aug, 2009.

- Joined King Fahd University of Petroleum and Minerals (KFUPM) in Feb, 2012.

Publications

- **K. Majeed**, S. Sorour, T. Y. Al-Naffouri, and S. Valaee, "Indoor localization using unsupervised manifold alignment with geometry perturbation," in IEEE WCNC14 Track 3 (Mobile and Wireless Networks) (IEEE WCNC14 Track 3 : NET), Istanbul, Turkey, Apr. 2014, pp. 2994-2999.